Loss-of-function mutations of CUL3, a high confidence gene for psychiatric disorders, lead to aberrant neurodevelopment in human induced pluripotent stem cells

Fischer, Sandra; Schlotthauer, Ines; Kizner, Valeria; Macartney, Thomas; Dorner-Ciossek, Cornelia; Gillardon, Frank

Published in:
Neuroscience

DOI:
10.1016/j.neuroscience.2020.08.028

Publication date:
2020

Journal Pre-proofs

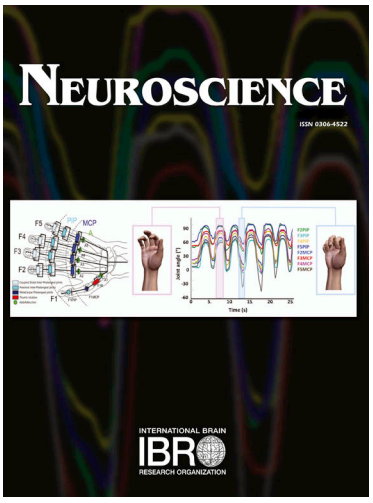

Loss-of-function mutations of CUL3, a high confidence gene for psychiatric disorders, lead to aberrant neurodevelopment in human induced pluripotent stem cells

Sandra Fischer, Ines Schlotthauer, Valeria Kizner, Thomas Macartney, Cornelia Dorner-Ciossek, Frank Gillardon

PII: S0306-4522(20)30545-5
DOI: https://doi.org/10.1016/j.neuroscience.2020.08.028
Reference: NSC 19845

To appear in: *Neuroscience*

Received Date: 16 March 2020
Revised Date: 25 July 2020
Accepted Date: 20 August 2020

Please cite this article as: S. Fischer, I. Schlotthauer, V. Kizner, T. Macartney, C. Dorner-Ciossek, F. Gillardon, Loss-of-function mutations of CUL3, a high confidence gene for psychiatric disorders, lead to aberrant neurodevelopment in human induced pluripotent stem cells, *Neuroscience* (2020), doi: https://doi.org/10.1016/j.neuroscience.2020.08.028

Supplementary Table S2. Summary of statistical analysis

Figure	Experiment	Test used	Statistic's value	P value
1B	CUL3 mRNA expression	Welch's ANOVA	W(4.00, 11.91) = 35.37	
	+/+_4 vs. +/-_6	Welch's t-test	t(8.15) = 5.27	0.0007
	+/+_2 vs. +/-_6	Welch's t-test	t(6.21) = 5.42	0.0015
	+/+_13 vs. +/-_6	Welch's t-test	t(9.82) = 4.26	0.0017
	+/+_4 vs. +/-_19	Welch's t-test	t(9.91) = 10.08	<0.0001
	+/+_2 vs. +/-_19	Welch's t-test	t(7.63) = 11.48	<0.0001
	+/+_13 vs. +/-_19	Welch's t-test	t(7.96) = 7.03	0.0001
2C	Cullin-3 protein expression	Welch's ANOVA	W(4.00, 7.32) = 6.31	
	+/+_4 vs. +/-_6	Welch's t-test	t(4.17) = 4.77	0.0080
	+/+_2 vs. +/-_6	Welch's t-test	t(5.27) = 4.27	0.0071
	+/+_13 vs. +/-_6	Welch's t-test	t(6.00) = 4.17	0.0059
	+/+_4 vs. +/-_19	Welch's t-test	t(5.30) = 3.05	0.0265
	+/+_2 vs. +/-_19	Welch's t-test	t(6.00) = 2.50	0.0469
	+/+_13 vs. +/-_19	Welch's t-test	t(5.16) = 2.60	0.0469
5A	PAX6 mRNA expression	Welch's ANOVA	W(4.00, 4.51) = 316.7	
	+/+_4 vs. +/-_6	Welch's t-test	t(2.20) = 34.92	0.0005
	+/+_2 vs. +/-_6	Welch's t-test	t(2.03) = 34.85	0.0007
	+/+_13 vs. +/-_6	Welch's t-test	t(2.14) = 38.48	0.0004
	+/+_4 vs. +/-_19	Welch's t-test	t(2.05) = 12.52	0.0057
	+/+_2 vs. +/-_19	Welch's t-test	t(2.01) = 12.17	0.0066
	+/+_13 vs. +/-_19	Welch's t-test	t(2.04) = 14.28	0.0045
5B	SLC1A3 mRNA expression	Welch's ANOVA	W(4.00, 4.67) = 5567	
	+/+_4 vs. +/-_6	Welch's t-test	t(2.01) = 21.98	0.0020
	+/+_2 vs. +/-_6	Welch's t-test	t(2.02) = 20.51	0.0022
	+/+_13 vs. +/-_6	Welch's t-test	t(2.00) = 21.15	0.0022
	+/+_4 vs. +/-_19	Welch's t-test	t(3.86) = 156.6	<0.0001
	+/+_2 vs. +/-_19	Welch's t-test	t(3.52) = 98.39	<0.0001
	+/+_13 vs. +/-_19	Welch's t-test	t(2.86) = 168.4	<0.0001
5C	Pax-6 positive cells	Welch's ANOVA	W(4.00, 4.42) = 41.98	
	+/+_4 vs. +/-_6	Welch's t-test	t(2.03) = 10.10	0.0092
	+/+_2 vs. +/-_6	Welch's t-test	t(2.00) = 10.54	0.0088
	+/+_13 vs. +/-_6	Welch's t-test	t(2.01) = 10.38	0.0090
	+/+_4 vs. +/-_19	Welch's t-test	t(2.61) = 8.13	0.0064
	+/+_2 vs. +/-_19	Welch's t-test	t(2.06) = 10.63	0.0079
	+/+_13 vs. +/-_19	Welch's t-test	t(2.30) = 9.65	0.0066
6A	MEA spike rate	two-way ANOVA		
		Interaction	F(2, 341) = 12.40	
		Row factor	F(2, 341) = 5.43	
		Column factor	F(1, 341) = 38.62	
	+/+_div19 vs. +/-_div19	Welch's t-test	t(56.35) = 5.11	<0.0001
	+/+_div23 vs. +/-_div23	Welch's t-test	t(48.39) = 6.64	<0.0001

Supplementary Table S2. Summary of statistical analysis (continued)

Figure	Experiment	Test used	Statistic's value	P value
8	Number of rosettes	Kruskal-Wallis	KW(5) = 214.9	
	+/+_4 vs. +/-_6	Mann-Whitney U	U(50,47) = 25	<0.0001
	+/+_2 vs. +/-_6	Mann-Whitney U	U(50,47) = 25	<0.0001
	+/+_13 vs. +/-_6	Mann-Whitney U	U(50,47) = 25	<0.0001
	+/+_4 vs. +/-_19	Mann-Whitney U	U(50,48) = 225	<0.0001
	+/+_2 vs. +/-_19	Mann-Whitney U	U(50,48) = 225	<0.0001
	+/+_13 vs. +/-_19	Mann-Whitney U	U(50,48) = 225	<0.0001
9B	Syn-1/2 positive puncta	Welch's ANOVA	W(4.00, 1197) = 760.8	
	+/+_4 vs. +/-_6	Welch's t-test	t(719.1) = 33.45	<0.0001
	+/+_2 vs. +/-_6	Welch's t-test	t(704.2) = 33.98	<0.0001
	+/+_13 vs. +/-_6	Welch's t-test	t(810.3) = 43.33	<0.0001
	+/+_4 vs. +/-_19	Welch's t-test	t(932.2) = 17.37	<0.0001
	+/+_2 vs. +/-_19	Welch's t-test	t(924.4) = 16.73	<0.0001
	+/+_13 vs. +/-_19	Welch's t-test	t(1033) = 23.97	<0.0001
10B	MEA spike rate	two-way ANOVA		
		Interaction	F (2, 102) = 8.224	
		Row factor	F (2, 102) = 215.3	
		Column factor	F (1, 102) = 25.28	
	+/+_2mA vs. +/-_2mA	Welch's t-test	t(21.09) = 3.09	0.0056
	+/+_5mA vs. +/-_5mA	Welch's t-test	t(23.93) = 4.07	0.0004
10C	Calcium imaging	two-way ANOVA		
		Interaction	F (4, 110) = 6.289	
		Row factor	F (4, 110) = 248.5	
		Column factor	F (1, 110) = 85.62	
	+/+_2Hz vs. +/-_2Hz	Welch's t-test	t(20.61) = 4.18	0.0004
	+/+_5Hz vs. +/-_5Hz	Welch's t-test	t(18.58) = 4.36	0.0004
	+/+_10Hz vs. +/-_10Hz	Welch's t-test	t(18.25) = 4.92	0.0001
	+/+_20Hz vs. +/-_20Hz	Welch's t-test	t(19.10) = 4.81	0.0001
	+/+_50Hz vs. +/-_50Hz	Welch's t-test	t(20.32) = 4.61	0.0002
11B	mRNA expression			
	+/+_SPRY1 vs. +/-_SPRY1	Welch's t-test	t(28.81) = 3.36	0.0022
	+/+_IL17RD vs. +/-_IL17RD	Welch's t-test	t(29.56) = 2.83	0.0083

Supplementary Table S1. Primary antibodies used for immunocytochemistry (ICC) or immunoblotting (IB).

Name	Species	Clonality	Dilution	Supplier	Cat. No.
Anti-Cullin-3	Mouse	Monoclonal	1:200 IB	Santa Cruz, Dallas, TX, USA	sc-166110
Anti-Cullin-3	Goat	Polyclonal	1:200 IB	Santa Cruz, Dallas, TX, USA	sc-8556

Anti-beta-Actin	Mouse	Monoclonal	1:3000 IB	Sigma-Aldrich, St. Louis, MO, USA	A5316
Anti-Oct-4	Rabbit	Monoclonal	1:400 ICC	Cell Signaling Technology, Danvers, MA, USA	2840
Anti-Tra-1-60	Mouse	Monoclonal	1:100 ICC	STEMCELL, Vancouver, Canada	60064
Anti-Pax-6	Rabbit	Polyclonal	1:100 ICC	Thermo Fisher Scientific, Waltham, MA, USA	42-6600
Anti-Map-2	Chicken	Polyclonal	1:1000 ICC	EnCor Biotechnology, Gainesville, FL, USA	CPCA-MAP2
Anti-vGlut-1	Mouse	Monoclonal	1:1000 ICC	Synaptic Systems, Goettingen, Germany	135511
Anti-Syn-1/2	Rabbit	Polyclonal	1:5000 ICC	Synaptic Systems, Goettingen, Germany	106002
Anti-Psd-95	Mouse	Monoclonal	1:100 ICC	Thermo Fisher Scientific, Waltham, MA, USA	MA1-046
Anti-RhoA	Mouse	Monoclonal	1:250 IB	Cytoskeleton, Denver, CO, USA	ARH04

Loss-of-function mutations of CUL3, a high confidence gene for psychiatric disorders, lead to aberrant neurodevelopment in human induced pluripotent stem cells

Sandra Fischer[1,*], Ines Schlotthauer[1,*], Valeria Kizner[1], Thomas Macartney[2], Cornelia Dorner-Ciossek[1], and Frank Gillardon[1]

[1]CNS Diseases Research, Boehringer Ingelheim Pharma GmbH & Co. KG, 88397 Biberach an der Riss, Germany

[2]MRC Protein Phosphorylation and Ubiquitylation Unit, Sir James Black Centre, University of Dundee, Dundee DD1 5EH, UK

*These authors contributed equally

Corresponding author:
Prof. Frank Gillardon, CNS Diseases Research, Boehringer Ingelheim Pharma GmbH & Co. KG, Birkendorfer Str. 65, 88397 Biberach an der Riss, Germany. Telephone: +49-7351-548460; e-mail: frank.gillardon@boehringer-ingelheim.com

Funding information
The research leading to these results has received support (one iPSC line from a healthy donor) from the Innovative Medicines Initiative Joint Undertaking under grant agreement n° 115439. Resources are composed of financial contribution from the European Union's Seventh Framework Program (FP7/2007-2013) and in kind contributions from EFPIA companies. This publication reflects only the author's views and neither the Innovative Medicines Initiative Joint Undertaking nor EFPIA nor the European Commission are liable for any use that may be made of the information contained therein.

Declarations of interest
Boehringer Ingelheim Pharma GmbH & Co. KG supported this work only by providing financial support in the form of authors' salaries and research materials. Study design, data analysis, decision to publish, and writing of the manuscript was performed independently. All authors declare no potential conflicts of interest.

Abstract

Both rare, high risk, loss-of-function mutations and common, low risk, genetic variants in the CUL3 gene are strongly associated with neuropsychiatric disorders. Network analyses of neuropsychiatric risk genes have shown high CUL3 expression in the prenatal human brain and an enrichment in neural precursor cells (NPCs) and cortical neurons. The role of CUL3 in human neurodevelopment however, is poorly understood. In the present study, we used CRISPR/Cas9 nickase to knockout CUL3 in human induced pluripotent stem cells (iPSCs). iPSCs were subsequently differentiated into cortical glutamatergic neurons using two different protocols and tested for structural/functional alterations. Immunocytochemical analysis and transcriptomic profiling revealed that pluripotency of heterozygous CUL3 knockout (KO) iPSCs remained unchanged compared to isogenic control iPSCs. Following small molecule-mediated differentiation into cortical glutamatergic neurons however, we detected a significant delay in transition from proliferating radial glia cells/NPCs to postmitotic neurons in CUL3 KO cultures. Notably, direct neural conversion of CUL3 KO iPSCs by lentiviral expression of Neurogenin-2 massively attenuated the neurodevelopmental delay. However, both optogenetic and electrical stimulation of induced neurons revealed decreased excitability in Cullin-3 deficient cultures, while basal synaptic transmission remained unchanged. Analysis of target gene expression pointed to alterations in FGF signaling in CUL3 KO NPCs, which is required for NPC proliferation and self-renewal, while RhoA and Notch signaling appeared unaffected. Our data provide first evidence for a major role of Cullin-3 in neuronal differentiation, and for neurodevelopmental deficits underlying neuropsychiatric disorders associated with CUL3 mutations.

Keywords: Neuropsychiatric disorders, CUL3, CRISPR/Cas9 nickase, induced pluripotent stem cells, human glutamatergic neurons, direct neuronal conversion

INTRODUCTION

Schizophrenia (SZ) is a severe neuropsychiatric disorder that affects about 21 million people worldwide and has a prevalence of approximately 1% (Lewis DA and Gonzalez-Burgos G, 2006; Millan MJ et al., 2016). SZ patients exhibit both positive symptoms (e.g. hallucinations, disorganized thought and speech), and negative symptoms, (e.g. cognitive impairments, social withdrawal) (Lewis DA and Gonzalez-Burgos G, 2006; Millan MJ et al., 2016). Since current medications mainly alleviate positive symptoms, there is a high unmet medical need for novel therapies targeting negative symptoms (reviewed in (Brennand KJ et al., 2011)). Environmental factors (e.g. stress in early life) increase the risk for SZ, but there is also a strong genetic component with a heritability of approximately 80% (Bahari-Javan S et al., 2017; Sullivan PF et al., 2003; Walsh T et al., 2008).

In 2014, a landmark genome-wide association study (GWAS) reported 108 schizophrenia-associated genomic loci representing low risk, common variants (Schizophrenia Working Group of the Psychiatric Genomics C, 2014). In this study, the CUL3 gene, which encodes the E3 ubiquitin ligase Cullin-3, was assigned to a non-coding risk locus by genomic proximity. In a more recent GWAS of schizophrenia, CUL3 was functionally annotated to non-coding genetic risk variants by chromatin conformation capture using both human brain tissue and iPSC-derived cortical neurons (Li M et al., 2018; Rajarajan P et al., 2018). Whether these non-coding risk variants increase or decrease CUL3 gene expression remains to be tested. The CUL3 gene is also affected by rare, high risk, *de novo* mutations in protein coding regions in patients diagnosed with SZ or autism spectrum disorder (ASD) (Lin GN et al., 2015). Moreover, CUL3 is listed as one of 23 high confidence risk genes for ASD in the SFARI Gene database (gene.safari.org/database). The E3 ubiquitin ligase Cullin-3 targets protein substrates for proteasomal degradation (reviewed in (Hershko A and Ciechanover A, 1998)). Cullin-3 binds to specific adaptor proteins that are important for recognition and ubiquitylation of protein substrates. Notably, protein-truncating, *de novo* mutations in CUL3 were detected in ASD patients, which disrupt Cullin-3 interaction with its adaptor, potassium channel tetramerization domain containing 13 protein (KCTD13) (Lin GN et al., 2015).

During the last decade, numerous iPSC lines were generated from patients diagnosed with various neuropsychiatric diseases. Differentiation of human iPSCs into forebrain neurons and subsequent structural/functional analyses contributed to a better understanding of the neurodevelopmental pathomechanisms that increase the risk for neuropsychiatric disorders (Brennand KJ et al., 2011; Marchetto MC et al., 2010; Murai K et al., 2016; Pasca SP et al., 2011; Sheridan SD et al., 2011). Several points are speaking in favor of CUL3 disease

modeling in iPSC-derived cortical glutamatergic neurons: (i) co-expression of CUL3 and its adaptor KCTD13 is high in the mid-fetal period of the developing human cortex (Kang HJ et al., 2011; Lin GN et al., 2015), (ii) the transcriptomic profile of human iPSC-derived neurons correlates best with that of human mid-fetal cortical neurons (Brennand K et al., 2015; van de Leemput J et al., 2014), and (iii) gene co-expression network analysis based on nine high confidence ASD risk genes including CUL3 showed convergence in mid-fetal cortical glutamatergic neurons (Willsey AJ et al., 2013). In the present study, we used CRISPR/Cas9 nickase to generate CUL3 knockout (KO) human iPSC lines and isogenic controls. This approach reduces off-target DNA cleavage observed with Cas9 nuclease (Ran FA et al., 2013), and minimizes the high variability observed with case/control iPSC lines carrying a different genetic background (Kyttala A et al., 2016). We differentiated the heterozygous CUL3 KO iPSC lines and the isogenic control iPSC lines into neural progenitor cells (NPCs) and cortical glutamatergic neurons using two protocols that others have employed to functionally assign non-coding SZ risk loci to causal genes by open chromatin profiling and chromatin interaction assays (Forrest MP et al., 2017; Rajarajan P et al., 2018). Small molecule-mediated neuronal differentiation revealed a massive delay in transition from proliferating radial glia cells/NPCs to postmitotic neurons in CUL3 KO cultures. This neurodevelopmental delay was not detectable by direct neuronal conversion of CUL3 KO iPSCs, however, induced Cullin-3 deficient neurons showed decreased excitability. Taken together, our study provides first evidence for a role of Cullin-3 ubiquitin ligase in human neurodevelopment and for potential neurodevelopmental deficits in psychiatric patients carrying CUL3 loss-of-function mutations.

EXPERIMENTAL PROCEDURES

Culture of human induced pluripotent stem cells

The quality-controlled (Sendai virus clearance, pluripotency, normal karyotype) human iPSC line SB Ad3 clone 4 (reprogrammed from skin fibroblasts of a 31 years old, healthy donor) was obtained from the StemBancc consortium (Kizner V et al., 2019; Morrison M et al., 2015). All iPSC lines were maintained under feeder-free conditions in Essential 8 medium (Gibco, Big Cabin, OK, USA) supplemented with 1:100 Antibiotic-Antimycotic (Life Technologies, Carlsbad, CA, USA). Cells were seeded on 6-well tissue culture plates (Sarstedt, Nümbrecht, Germany) coated with Matrigel basement membrane matrix (Corning, Corning, NY, USA). Matrigel was diluted 1:10 in DMEM/F12 and Glutamax (Gibco, Big Cabin, OK, USA). Cells were split before reaching 100% confluence using 0.02% EDTA (Sigma-Aldrich, St. Louis, MO, USA) and were replated in E8 medium supplemented with 10 µM ROCK inhibitor Y27632 (Tocris, Bristol,

United Kingdom). Cells were cultured at 37°C and 5% CO_2. All iPSC lines and iPSC-derived cells were negatively tested for mycoplasma using MycoAlert™ PLUS Mycoplasma Detection Kit (Lonza, Basel, Switzerland) according to the manufacturer's protocol.

Genome editing using CRISPR/Cas9 D10A nickase

The human iPSC line SB Ad3 clone 4 (abbreviated CB4) (Morrison M et al., 2015) was used for CUL3 gene knockout by Cas9 D10A nickase and two guide RNAs (gRNAs). The gRNAs were identified using the Sanger Institute CRISPR webtool (http://www.sanger.ac.uk/htgt/wge/find_crisprs) and chosen on the basis of having the lowest combined off-targeting score whilst targeting as many of the known and predicted transcripts as possible. Since there exists no off target pairing of these gRNAs closer than 1kb to one another, we consider the possibility of off-target DNA cleavage to be negligible. Both gRNAs target exon 5 of the CUL3 gene. The antisense guide 5'-GACCTAAAATCATTAACATC-3' was cloned into the spCas9 D10A nickase expressing vector pX335 and the sense guide 5'-GAGTCTATGAAGAAGATTTTG-3' into the puromycin selectable plasmid pBABED P U6. Human iPSCs were grown to 80% confluency and treated with 10 µM ROCK inhibitor Y27632 one day prior to nucleofection. Cells were dissociated into single cells using 0.5 ml Accutase (Merck). 5 µg of each plasmid were mixed with the nucleofection solution of the Amaxa Human Stem Cell Nucleofector Starter Kit (Lonza, Basel, Switzerland). Nucleofection was performed using program B-016 of the Amaxa nucleofector device. Nucleofected iPSCs were seeded on Matrigel-coated 10 cm cell culture dishes containing E8 medium and 10 µM ROCK inhibitor Y27632. After 24 hours, medium was changed to E8 supplemented with 0.5 µg/ml puromycin (Merck, Darmstadt, Germany) for 3 days and replaced daily. Puromycin resistant single iPSC colonies were picked and expanded under iPSC maintenance conditions.

T7 Endonuclease Assay

Formation of insertions/deletions following Cas9 D10A nicking in the CUL3 exon 5 region was tested using T7 Endonuclease assay according to the protocol of the EnGen Mutation Detection Kit (New England Biolabs, Ipswich, MA, USA). DNA of iPSC clones was extracted using QuickExtract™ DNA Extraction Solution 1.0 according to the manufacturer's protocol (Epicentre, Madison, WI, USA). Genomic regions encompassing the gRNA target sites were amplified using forward primer 5'-GCTGCAGCTAAAGTGGCTTG-3' and reverse primer 5'-AGCCTGCAGATGAGACTTCG-3'. Annealing temperature was calculated using Tm calculator from New England Biolabs (https://www.neb.com/). PCR amplification was performed using the following cycling conditions: 1 cycle for 30 seconds at 98°C, 35 cycles for 5, 10 and 50 seconds at 98°C, 65°C and 72°C respectively, followed by 1 cycle for 7 minutes at 72°C. PCR

products were electrophoretically separated on a 2% E-Gel Precast Agarose Gel stained with ethidium bromide (Thermo Fisher Scientific, Waltham, MA, USA) on an E-Gel iBaseTM Power System device (2 min of PRE-RUN and program 1E-Gel 0.8-2%) for 26 min. Images were analyzed using the ChemiDoc gel imaging system (Bio-Rad, Hercules, CA, USA). Fragment analysis considered samples with only one full-length, non-cleaved band as negative clones, whereas more than two bands indicate insertion/deletion formation following Cas9 D10A nicking.

Karyotype analysis

DNA was extracted from nucleofected iPSC clones using Qiagen AllPrep DNA/RNA Micro Kits according to the manufacturer's protocol (Qiagen, Hilden, Germany). DNA samples were sent to Life & Brain Genomics (Bonn, Germany) for karyotype analysis using the Illumina BeadArray Technology (HumanOmni2.5Exome-8 BeadChip v1.3, Illumina, San Diego, CA, USA). Genotypes were analyzed using GenomeStudio V2.0.2. For copy number analysis, the CNV-Partition algorithm version 3.2 (Illumina, San Diego, CA, USA) was applied. Copy number variants were reported, if larger than 350.000 base pairs.

DNA sequencing

Genomic DNA encompassing the gRNA target sites was amplified using HotStart Q5 Polymerase (New England Biolabs, Ipswich, MA, USA). PCR products were custom sequenced by Sequiserve (Munich, Germany).

Neuronal differentiation of iPSCs using small molecules

Differentiation of iPSCs into neural progenitor cells (NPCs) and cortical glutamatergic neurons was based on a well-established protocol (Shi Y et al., 2012; Shi Y et al., 2012), which others have employed to assign non-coding SZ risk variants to causal genes by open chromatin profiling (Forrest MP et al., 2017). Neural induction was initiated by incubating iPSCs (at approximately 90% confluency) for 8-12 days with Neural Induction Medium consisting of 250 ml DMEM/F12 and GlutaMAX™ medium, 250 ml Neurobasal™ medium, 1.25 mg Insulin (Sigma-Aldrich, St. Louis, MO, USA), 2.5 ml Sodium Pyruvate (Sigma-Aldrich, St. Louis, MO, USA), 0.5 ml beta-mercaptoethanol, 2.5 ml Non-Essential Amino Acids Solution (100x), 1.25 ml PenStrep, 2.5 ml N2 supplement (100x), 5 ml B-27™ supplement (50x, serum free), 2.5 ml L-Glutamine (all Thermo Fisher Scientific, Waltham, MA, USA), 1 µM Dorsomorphin and 10 µM SB431542 (both Merck, Darmstadt, Germany). Neuroepithelial sheets were dissociated with 10 mg/ml Dispase (Thermo Fisher Scientific, Waltham, MA, USA) on day 8 and replated on laminin-coated (Sigma-Aldrich, St. Louis, MO, USA) 6 well plates. On day 13, neural rosette

formation was promoted by adding medium with 20 ng/ml FGF2 (R&D Systems, Minneapolis, MN, USA) for 4 days. Non-neuronal differentiation was reduced by multiple dissociation steps using 10 mg/ml Dispase. From day 17 to 25 medium was exchanged every second day. On day 25, NPCs were dissociated into single cells using Accutase (Merck, Darmstadt, Germany). For differentiation into cortical neurons, NPCs were seeded on 2x concentrated Matrigel plates. Cells were cultured in medium containing 10 µM DAPT (STEMCELL, Vancouver, Canada), 50 µM cAMP, 20 ng/ml BDNF and 20 ng/ml GDNF (both PeproTech, Rocky Hill, NJ, USA) for four days and subsequently replated on assay plates coated with 0.07% polyethyleneimine (Sigma-Aldrich, St. Louis, MO, USA) in borate buffer and 1:100 laminin (Sigma-Aldrich, St. Louis, MO, USA). For neuronal maturation, DAPT was omitted and medium containing 50 µM cAMP, 20 ng/ml BDNF and 20 ng/ml GDNF was exchanged three times per week.

Direct neuronal conversion of iPSCs using lentiviral NGN2 expression

Human iPSCs were directly converted into glutamatergic cortical neurons by tetracycline-inducible expression of the neuralizing transcription factor Neurogenin-2 (NGN2) following lentiviral transduction as originally described by Zhang et al (Zhang Y et al., 2013). Lentiviral production was performed as described elsewhere (Colasante G et al., 2015). For accelerated induction of excitatory neurons, we combined direct NGN2-mediated conversion with developmental pattering, as recently reported by others (Nehme R et al., 2018; Qi Y et al., 2017). Human iPSC were patterned towards a dorsal forebrain phenotype by pharmacological inhibition of TGF-beta, BMP, and WNT signaling using SB431542 (10 µM), LDN193189 (250 nM), and XAV939 (5 µM). To accelerate neuronal fate acquisition, we additionally inhibited FGF, Notch, and MEK signaling using SU5402 (10 µM), DAPT (10 µM), and PD0325901 (8 µM). Induced neurons were replated and cocultured with rat primary cortical astrocytes (Thermo Fisher Scientific, Waltham, MA, USA) on day 8 post transduction in order to promote neuronal maturation and synapse formation (Zhang Y et al., 2013).

Quantitative real time PCR (qRT-PCR)

Cells were lysed in RLT buffer (Qiagen, Hilden, Germany) supplemented with 1% beta-mercaptoethanol (Carl Roth, Karlsruhe, Germany). Lysates were homogenised using QIAshredder columns (Qiagen, Hilden, Germany) and total RNA was extracted using RNeasy Mini Kit (Qiagen, Hilden, Germany) as described in the manufacturer's protocol including an on-column DNase digestion step. RNA concentration and quality were analyzed using a NanoDrop 1000 device (Thermo Fisher Scientific, Waltham, MA, USA). RNA was reverse transcribed to cDNA using SuperScript VILO cDNA Synthesis Kit (Invitrogen, Carlsbad, CA,

USA) according to manufacturer's protocol. For PCR analysis triplicates of cDNA samples were amplified using TaqMan Gene Expression Assay (Thermo Fisher Scientific, Waltham, MA, USA and QuantiFast Probe RT-PCR MasterMix (Qiagen, Hilden, Germany). Validated primer pairs for human transcripts were acquired from Thermo Fisher Scientific (Waltham, MA, USA). The CUL3 primer pair binds on the exon 14-15 boundary. PCR data were analyzed using QuantStudio™ 6 Flex Real-Time PCR System (Applied Biosystems, Foster City, CA, USA). Samples were normalised to the housekeeping gene POLR2A and evaluated by the $\Delta\Delta C_T$ method.

Immunocytochemical analysis

Cells were fixed in 4% paraformaldehyde (Sigma-Aldrich, St. Louis, MO, USA) in phosphate-buffered saline (PBS) for 15 minutes at room temperature. After three washing steps, cells were permeabilized in 0.1% Triton X-100 (Sigma-Aldrich, St. Louis, MO, USA) for 15 minutes. Unspecific protein binding was blocked in 5% Normal Goat Serum (Cell Signaling Technology, Danvers, MA, USA) at room temperature for 2 hours. Primary antibodies were diluted in 10% Fetal Bovine Serum (Gibco, Big Cabin, OK, USA) and incubated over night at 4°C. Primary antibodies used for immunocytochemistry are listed in Supplementary Table 1. Alexa-conjugated secondary antibodies were diluted in 5% Fetal Bovine Serum and incubated for 2 hours at room temperature, protected from light. Hoechst 33342 dye (1:2000 in PBS) (Molecular Probes, Eugene, OR, USA) was used to stain nuclei. For detection of the fluorescent signals, the Opera Phenix™ High-Content Screening System (PerkinElmer, Waltham, MA, USA) at 20x or 63x magnification was used. Digital images were analyzed using Columbus software (Version 2.7.0.130974, PerkinElmer, Waltham, MA, USA) as described in detail elsewhere (Kizner V et al., 2019). Dead cells showing condensed/fragmented nuclei were excluded from analysis. The ratio of immunofluorescent cells to viable cells (Hoechst-positive, non-condensed/non-fragmented nuclei) was calculated to evaluate the percentage of immunopositive cells.

Immunoblot analysis

Cells were lysed in Cell Lysis Buffer (Cell Signaling Technology, Danvers, MA, USA) supplemented with 1:100 protease inhibitor cocktail and phosphatase inhibitor cocktail 2 (both Sigma). Samples were incubated on ice for 15-20 min. Subsequently, cell debris was pelleted by centrifugation at 21000xg for 10 min at 4°C, and supernatants were used for further analysis. Protein concentrations were determined using BioRad Assay Dye Reagent and a microplate reader Wallac Victor (Perkin Elmer). Briefly, 10 µl of BSA protein standards and 10 µl protein samples (diluted 1:10 in ddH2O) were added to a 96-well plate. 200 µl BioRad Assay Dye

Reagent was added and incubated for 5 min in the dark. Plate was measured and protein concentration was calculated using Excel and GraphPad Prism. SDS gel-electrophoresis of protein lysates was performed using NuPAGE™ 4-12% Bis-Tris Protein Gels (Life Technologies, Carlsbad, CA, USA) at 200 V for 45 minutes in 3-(N-morpholino)propanesulfonic acid (MOPS) buffer (Invitrogen, Carlsbad, CA, USA). Proteins were transferred to a nitrocellulose membrane in Tris-Glycine Buffer (Bio-Rad, Hercules, CA, USA) supplemented with 20% methanol at 100 V for 90 minutes. MemCode Reversible Protein Stain (Thermo Fisher Scientific, Waltham, MA, USA) was used to assess equal protein loading. Membranes were blocked with 5% milk powder in TBS and 0.1% Tween20 (TBST) for 2 hours followed by incubation with primary antibodies at 4°C overnight. Primary antibodies are listed in Supplementary Table 1. HRP-conjugated secondary antibodies were added for 2 hours, and protein bands were visualised by enhanced chemiluminescence using Western Lightning Plus-ECL reagent (PerkinElmer, Waltham, MA, USA). Some blot membranes were stripped using Pierce Restore Western Blot Stripping Buffer (Thermo Fisher Scientific, Waltham, MA, USA) for 15 min at room temperature, washed in TBST, blocked and incubated with antibodies as described above. Blots were imaged using a ChemiDoc Imaging System (Bio-Rad, Hercules, CA, USA) and volume band intensity was quantified using ImageLab Software (Bio-Rad, Hercules, CA, USA).

Modeling of protein structure

Modeling of 3-dimensional protein structure was based on the amino acid sequence of Cullin-3 protein available from from UniProt Knowledgebase (http://www.uniprot.org/uniprot/Q13618), the protein structure homology-modeling software from SWISS-MODEL (https://swissmodel.expasy.org/interactive) (Waterhouse A et al., 2018) and the molecular visualisation software PyMOL (The PyMOL Molecular Graphics System, Version 2.0 Schrödinger, LLC).

EdU labeling of proliferating cells

Click-iT EdU Imaging Kit including Alexa Fluor® 488, 594 and 647 Azides (Life Technologies, Carlsbad, CA, USA) was used according to the manufacturer's protocol. 20 µM EdU solution was added to proliferating iPSCs/NPCs and incubated at 37°C for 60 minutes. Cells were fixed in 4% PFA for 15 minutes at room temperature, followed by permeabilisation in 0.5% Triton X-100 for 20 minutes. Click-iT reaction cocktail was added to each well and incubated for 30 minutes, protected from light. Hoechst 33342 (1:16000 in PBS) was added for nuclear DNA counterstaining. Detection of EdU positive cells was performed using Opera Phenix™ High-Content Screening System (PerkinElmer, Waltham, MA, USA) (20x water objective and

channels Alexa488, Alexa594, Alexa647 and DAPI). Images were analyzed using Columbus software and the ratios of EdU-positive proliferating cells to Hoechst-positive total cells were calculated.

PCR Array analyses

To analyze expression of genes regulating human neurogenesis, RT² Profiler™ PCR Arrays Human Neurogenesis (Qiagen, Hilden, Germany, Format A) were used as described in the PCR array handbook (http://www.sabiosciences.com/Manual/1070190.pdf). RNA was extracted from NPC lysates using RNeasy Mini Kits (Qiagen, Hilden, Germany). Reverse transcription to cDNA was performed using RT^2 First Strand Kit (Qiagen, Hilden, Germany). A genomic DNA elimination mix was added to 500 ng RNA and incubated for 5 minutes at 42°C followed by 1 minute on ice. Reverse-transcription mix was then added to the genomic DNA elimination mix and incubated for another 15 minutes at 42°C. Reaction was stopped by incubation at 95°C for 5 minutes. 2xRT^2 SYBR Green Mastermix and RNase-free-water were added to the cDNA. Real-time PCR was performed using QuantStudio 6k Flex (Applied Biosystems, Foster City, CA, USA). Cycling conditions were as follows: 1 cycle for 10 minutes at 95°C, and 40 cycles with 15 seconds (95°C) and 1 minute (60°C). Baseline settings were calculated automatically, whereas the threshold (ΔRn vs cycle) was manually set to 0.05. Gene expression was analyzed using the $\Delta\Delta C_T$-method and the online Qiagen software tool (www.sabiosciences.com/pcrdataanalysis.php). The C_T cut-off was set to 30. Genes with a fold-regulation greater than 2 or smaller than -2 compared to the wildtype clones were considered as deregulated. P-values were calculated by comparing the three wildtype clones versus the three CUL3 knockdown clones, and p-value threshold was set to 0.1.

To analyze expression of human genes encoding neurotransmitter receptors/transporters, TaqMan™ Arrays Human Neurotransmitters (Applied Biosystems, Foster City, CA, USA) were used according to the manufacturer's manual (https://assets.thermofisher.com/TFS-Assets/LSG/manuals/cms_053406.pdf). Sample preparations and experimental procedures were performed as described in the PCR array handbook (http://www.sabiosciences.com/Manual/1070190.pdf) and below. Post-mitotic neurons derived from iPSCs were lysed in RLT-buffer supplemented with 1% beta-mercaptoethanol after 16 days of maturation. RNA was extracted using RNeasy Micro Kit according to the manufacturer's protocol (Qiagen, Hilden, Germany). Transcription to cDNA was performed as described in the manual of the High-Capacity cDNA Reverse Transcription Kit (Applied Biosystems, Foster City, CA, USA). TaqMan Gene Expression Master Mix (Thermo Fisher Scientific, Waltham, MA, USA) was added to the cDNA samples. Real-time PCR was performed using QuantStudio 6k Flex (Applied Biosystems, Foster City, CA, USA). Cycling

conditions and instrument settings are described in the Neurogenesis PCR Array chapter above. For data evaluation, C_T-values were exported to Excel and analyzed using the $\Delta\Delta C_T$-method. The C_T cut-off was set to 30. Genes with a fold-regulation greater than 2 or smaller than -2 compared to the wildtype clones were considered as deregulated. P-values were calculated by comparing the three wildtype clones versus the three knockdown clones and p-value threshold was set to 0.05.

Multi-electrode array recordings and optogenetic stimulation

Multi-electrode array (MEA) plates (24-well, Multi Channel Systems MCS, Reutlingen, Germany) were coated by adding 100 µl polyethylenimine solution (0.07%) per well and incubating for 1h at 37°C. Plates were rinsed twice with PBS and water and dried overnight. On the following day, neurons were dot-seeded on the electrode area at a density of 120,000 cells per well in 10 µl medium containing 80 µg/ml laminin. After 1h incubation at 37°C, medium volume was increased to 500 µl. A 50% medium exchange was performed every 2-3 days. Spontaneous extracellular field potentials were recorded at 37°C under a 5% CO_2 atmosphere using the Multiwell-MEA system and Multiwell Screen software (Multi Channel Systems MCS, Reutlingen, Germany). After an equilibration period of 5 min, recordings were performed for 10 min at a sampling rate of 20 kHz. A 10 Hz to 2.5 kHz bandwidth filter was applied. Data analysis was performed using Multiwell Analyzer software (Multi Channel Systems MCS, Reutlingen, Germany). Spikes were counted, if the recorded signal exceeded a threshold of 5 times the standard deviation of the baseline noise level. Electrodes were considered active, if the spike rate exceeded 0.1 Hz. A burst was defined as a series of at least 7 consecutive spikes with a maximum inter-spike interval of 50 ms. Network bursts were counted, if a minimum of 8 out of 12 electrodes per well recorded simultaneous burst-firing. Multiparametric analysis of spikes, bursts and network bursts was performed using Microsoft Excel (Microsoft Corporation, Redmond, WA, USA) and GraphPad Prism 8 (GraphPad Software, San Diego, CA, USA). For artifact-free, precise stimulation, iPSCs were transduced both with a lentiviral vector encoding channelrhodopsin-2 (ChR2), a light-gated cation channel (Nagel, PNAS, 2003), tagged with a fluorescent EYFP reporter and with lentiviral NGN2. On day 34 of neuronal maturation, brief (50 ms) blue light pulses (470 nm) were applied to ChR2 expressing neurons by a 3x24 light emitting diodes (LEDs) carrying device (LED stimulator MW24-opto-stim, Multi Channel Systems MCS, Reutlingen, Germany) that was positioned onto the MEA plate. Light intensity was modulated by applying pulses at controlled currents ranging from 2 mA to 5 mA (Multiwell-Screen software, Multi Channel Systems MCS, Reutlingen, Germany).

Calcium imaging

Calcium imaging was performed using a fluorometric imaging plate reader (FLIPR Tetra, Molecular Devices, San Jose, CA, USA). Neurons were seeded into 384-well plates coated with poly-L-lysine, laminin and fibronectin (all Sigma-Aldrich, St. Louis, MO, USA) at a density of 5000 cells per well on day 8 post transduction. After three weeks of maturation, the plates were carefully washed with Ringer buffer consisting of 130 mM NaCl, 5 mM KCl, 1 mM $CaCl_2$, 1 mM $MgCl_2$, 2 mM KH_2PO4, 20 mM HEPES and 5 mM glucose at pH 7.4. Measurements of intracellular calcium were performed after 1 hour incubation with Calcium 4 assay reagent (Molecular Devices, San Jose, CA, USA). Briefly, 1 minute baseline recording was followed by stepwise electrical stimulation at a constant voltage of 12V with 5 seconds stimulation each at 2, 5, 10, 20 and 50 Hz in 2-minute intervals. Neuronal excitability was calculated by subtracting the baseline signal from maximal relative light units in response to electrical stimulation and normalizing the resulting value to the baseline.

Statistical analysis

Biological assays were performed using the wildtype parental iPSC line and two heterozygous CUL3 knockout iPSC lines showing different deletions. In addition, two iPSC lines, which went through nucleofection and selection, but did not show genomic modifications, were included as controls. No statistical methods were used to predetermine sample size. However, the sample sizes in our study are similar to those reported in previous publications (Brennand KJ et al., 2011; Kizner V et al., 2019; Pak C et al., 2015) that showed significance. The sample sizes and the description of the sample collection are reported in the figure legends. For MEA recordings, FLIPR-based calcium imaging, and high-content microscopic screening, the cells were randomly assigned to the cell culture plates. For subsequent data acquisition, investigators were blinded with regard to the group category.

Graph Pad Prism version 8 (GraphPad Software, San Diego, USA) was used for all statistical analyses and graphing. Inferential statistical strategies of continuous variables are based on parametric one-factorial or two- factorial linear models (Welch's ANOVA or two-way ANOVA) followed by pairwise comparisons using a t-test modification according to Welch to account for unequal standard deviations in both groups. Discrete count data are analyzed using a non-parametric, rank-based Kruskal-Wallis test followed by pairwise Mann-Whitney U tests.

The significance level is set to 5% per hypothesis. P values in the figures are presented as follows: *$p \leq 0.05$, **$p \leq 0.01$, ***$p \leq 0.001$, ****$p \leq 0.0001$. Data are shown as mean ± standard error of the mean (SEM). In box-and whiskers plots the box depicts the median and the 25th and 75th quartiles, and the whiskers show the 5th and 95th percentile. Additional information on statistical analysis (e.g. degrees of freedom, statistic's values, exact p-values) is given in Supplementary Table S2.

RESULTS

Generation of CUL3 knockout iPSC lines and isogenic controls

CUL3 is a high risk gene for neuropsychiatric disorders (Codina-Sola M et al., 2015; Schizophrenia Working Group of the Psychiatric Genomics C, 2014), but little is known about its function in human neurons. To get a better insight into the role of CUL3 in human neurodevelopment, we investigated the consequences of CUL3 knockout (KO) in human iPSC and iPSC-derived cortical neurons. We used CRISPR/Cas9-mediated genome modification, which enables the generation of isogenic iPSC lines, thereby reducing genetic background heterogeneity and experimental variability (Jinek M et al., 2012; Kim HS et al., 2014). We selected the human iPSC line SB Ad3 clone 4 (abbreviated CB4), which has been generated and validated by the StemBancc consortium (Morrison M et al., 2015). Human iPSCs were nucleofected with plasmid vectors encoding Cas9 D10A nickase (Cas9n) and antisense gRNAs targeting exon 5 of the CUL3 gene. The Cas9n double-nicking approach was chosen, in order to increase target specificity and reduce off-target effects as shown by others (Ran FA et al., 2013). Guide RNA off-target analysis revealed 10 potentials off-targets showing ≥ 3 mismatches and a low score. Importantly, there is no off-target pairing of these gRNAs closer than 1 kb to one another, such that the possibility of off-target DNA cleavage is considered to be negligible.

Following nucleofection and puromycin selection, iPSC clones carrying CRISPR/Cas9n-mediated insertions/deletions were identified by T7 endonuclease assay (Fig. 1A). Only iPSC clones showing a normal karyotype were included in subsequent analyses. By genomic DNA sequencing we detected a 3 base pair (bp) deletion in the heterozygous CUL3 KO iPSC clone 6, and a 17 bp deletion in the heterozygous CUL3 KO iPSC clone 19 (Fig. 1C). According to UniProt Knowledgebase, either amino acid Glu202 or Glu203 of human Cullin-3 protein (Q13618) was deleted in clone 6. The 17 bp frameshift deletion in clone 19 is predicted to lead to a premature stop codon following amino acid 199 (p.Phe199X), which may result in nonsense-mediated mRNA decay (Chang YF et al., 2007) of the mutant transcript, or translation of a truncated, likely inactive Cullin-3 protein fragment from the mutant allele. Cullin-3 has an N-terminal domain that comprises three repeats with five alpha-helix bundles each (Petroski MD and Deshaies RJ, 2005). Our modeling of the 3-dimensional protein structure of Cullin-3 using SWISS-MODEL and PyMOL software revealed that amino acids 202/203 are located in alpha-helix C of repeat 2 of the Cullin-repeat motif (Petroski MD and Deshaies RJ,

2005; Zheng N et al., 2002). Uniprot Knowledgebase also showed that amino acids Glu202 and Glu203 are highly conserved between species. Moreover, a potentially deleterious, in-frame deletion of Glu203 (variant 2:225378283 p.Glu203del) in human Cullin-3 has been reported by the Exome Aggregation Consortium (Lek M et al., 2016). Similar to CUL3 gene targeting in mice (Singer JD et al., 1999), we did not detect a homozygous CUL3 KO clone. In addition to the wildtype parental iPSC line CB4, two iPSC clones (clone 2 and clone 13), which went through CRISPR/Cas9 nucleofection, but did not show insertions/deletions, were included as controls in subsequent analyses.

Quantitative real-time polymerase chain reaction (qRT-PCR) confirmed an approximately 50% decrease in CUL3 mRNA expression in heterozygous CUL3 KO iPSC clones (Fig. 1B). Consistently, Cullin-3 protein levels were significantly reduced in heterozygous CUL3 KO iPSCs, as shown by immunoblot analyses using both a monoclonal anti-Cullin-3 antibody against the N-terminus of human Cullin-3, and a polyclonal anti-Cullin-3 antibody against the C-terminus (Fig. 2). In protein lysates from heterozygous CUL3 KO clone 19, a truncated Cullin-3 protein fragment was not detected, and the Cullin-3 protein band was shifted towards a slightly higher molecular weight (Fig. 2A). In addition, by total protein staining of the blots we did not detect protein bands with increased intensity in the heterozygous CUL3 KO iPSC lines (Fig. 2A). This suggests that a heterozygous loss of CUL3 has a moderate effect on protein ubiquitination/degradation, or that Cullin-3 preferentially acts on low abundance proteins that are not detectable by our protein stain.

CUL3 deficiency does not affect stemness of human iPSCs

Since CUL3 is highly expressed in human iPSCs (Fig. 1B) (van de Leemput J et al., 2014), we investigated its potential role in stemness by immunostaining for marker proteins. Expression of the cell surface protein Tra1-60 and the nuclear protein Oct-4 was assessed in iPSC cultures by high-content digital image analysis (Fig. 3). More than 98% of the iPSCs were immunopositive for Oct-4 both in heterozygous CUL3 KO cultures (clones 6 and 19) and in isogenic controls (clones CB4, 2, and 13) (n = 11 wells per clone). Percentage of Tra1-60 immunopositive cells did not significantly differ between the genotypes as well. Furthermore, high-content image analysis of the percentage of viable iPS cells showing Hoechst-positive, non-condensed/non-fragmented nuclei did not show significant differences between the genotypes, which indicates that cell viability and proliferation are unaltered.

NPCs differentiated from heterozygous CUL3 knockout iPSCs exhibit a moderate increase in cell proliferation

CUL3 deficiency in mouse embryonic fibroblasts resulted in an increased percentage of cells in S phase of the cell cycle (McEvoy JD et al., 2007). To examine the effect of CUL3 deficiency on proliferation of human iPSCs and NPCs, we analyzed incorporation of 5-ethynyl-2-deoxyuridine (EdU) during DNA replication by high-content image analysis of cell cultures. The percentage of iPSCs showing EdU-positive nuclei showed a trend ($p > 0.05$) towards increased proliferation in the two heterozygous CUL3 KO clones compared to isogenic wildtype control clones (Fig. 4B). The percentage of NPCs showing EdU-positive nuclei was moderately, but significantly increased in the two heterozygous CUL3 KO clones compared to isogenic wildtype controls (Fig. 4B). Similar iPS cell proliferation and iPS cell density between the genotypes make an indirect effect on neural cell-fate commitment (Chambers SM et al., 2009) unlikely.

PCR array analyses reveal increased mRNA expression of PAX6 in heterozygous CUL3 KO NPC cultures and altered mRNA expression of neurotransmitter receptor/transporters in CUL3 KO neurons

To assess a potential function of Cullin-3 in human neurodevelopment more broadly, we analyzed mRNA expression of 84 genes regulating neurodevelopment using 96-well RT^2 Profiler PCR Arrays Human Neurogenesis. RNA extracts from the five NPC clones were analyzed using one PCR array each as described in detail in the Experimental Procedures section. Data analysis using the manufacturer's online software showed a 5-fold and 4-fold increase in PAX6 mRNA levels in heterozygous CUL3 KO clones 6 and 19, respectively (Fig. 5A), whereas expression of TENM1 mRNA decreased 2-fold. All other arrayed genes were not differentially expressed at a C_T cut-off of 35 and a p-value threshold of 0.1. Since PCR array analysis generated only a single data point per transcript, we subsequently analyzed PAX6 mRNA expression by qRT-PCR in order to demonstrate statistical significance. Consistent with data from PCR array analysis, PAX6 mRNA levels significantly increased approximately 3-fold in heterozygous CUL3 KO clones 6 and 9 compared to isogenic wildtype clones (Fig. 5A). Immunostaining of NPC cultures and digital image analysis also showed increased numbers of strongly Pax-6 immunofluorescent nuclei in heterozygous CUL3 KO clones, whereas Nestin immunofluorescence was unchanged (Fig. 5C).

Next, we analyzed expression of 92 neurotransmitter receptors/transporters in iPSC-derived cortical neurons after 2 weeks of differentiation/maturation using 96-well qPCR Arrays Human Neurotransmitter (as described in detail in the Experimental Procedures section). Data analysis using the manufacturer's online software revealed a significant (p-value threshold 0.05) decrease in mRNA levels of the gamma-aminobutyric acid type A receptor gamma 1 subunit (GABRG1), and the serotonin receptor 5-hydroxytryptamine receptor 2A (HTR2A) in heterozygous CUL3 KO iPSC-derived neurons. Notably, mRNA expression of the glutamate

transporter solute carrier family 1 member 3 (SLC1A3/EAAT1/GLAST1) showed a significant increase in CUL3 KO neuron cultures, which we confirmed by qRT-PCR (Fig. 5B). In the adult human brain, SLC1A3 is preferentially expressed in mature astrocytes (Hertz L and Zielke HR, 2004), whereas in the developing human neocortex, SLC1A3 is expressed in proliferating radial glia cells (RGCs) and NPCs (Polioudakis D et al., 2019; Zhong S et al., 2018). Since GFAP-immunopositive astrocytes become detectable only after about 6 weeks of small molecule differentiation of human iPSCs *in vitro* ((Shi Y et al., 2012) and present study), higher levels of the RGC/NPC marker PAX6 and SLC1A3 versus lower levels of neurotransmitter receptors may indicate a delay in transition from proliferating RGCs/NPCs to postmitotic neurons in CUL3 KO cultures. Higher PAX6 mRNA expression in CUL3 KO NPCs might also indicate an enhanced pallial fate in mutant NPCs. However, this seems unlikely, since mRNA levels of the pallial marker gene LHX2 (96.1% ± 4.8%) and the subpallial marker gene DLX1 (107.3% ± 10.4%) were not significantly altered in heterozygous CUL3 KO NPC cultures compared to isogenic controls.

CUL3 KO neuron cultures exhibit a decrease in spontaneous neuronal network activity and an appearance of neural rosettes following small molecule-mediated differentiation from iPSC

To test neuronal function, we dot-seeded iPSC-derived immature neurons onto 24-well glass-bottom, multi-electrode array (MEA) plates containing 12 electrodes per well. We recorded spontaneous electrical activity starting at day-in-vitro (div) 12 after seeding onto MEA plates, when action potential firing becomes detectable (Shi Y et al., 2012). At div 12 spike rate did not significantly differ between heterozygous CUL3 KO neuron cultures and isogenic wildtype controls (Fig. 6A). At div 23 spike rate in wildtype neuron cultures showed a trend towards an increase. Since neuronal differentiation/maturation using small molecules follows a more protracted time-course (Shi Y et al., 2012), this increase might become significant only at later time-points. More importantly, between div 19 and div 23 after seeding, we detected a massive decline in neuronal activity in the heterozygous CUL3 KO cultures. Bright-field microcopy of the glass-bottom MEA plates revealed the presence of numerous, radial-symmetric neural rosettes in CUL3 KO neuron cultures (inset Fig. 6A), which were not visible in isogenic controls. It may be hypothesized that these proliferating RGCs/NPCs overgrow the neuron cultures over time, and cause a decline in MEA signals by blocking contact to electrodes and/or by competing with neurons for essential medium nutrients.

To confirm appearance of neural rosettes composed of RGCs/NPCs during maturation of CUL3 KO iPSC-derived neurons, we performed small molecule-mediated neuronal differentiation of our iPSC lines on 96-well plates. Following immunostaining for the NPC

marker Pax-6 and the neuronal marker Map-2 at div 23 after replating, we detected numerous Pax-6 immunopositive RGCs/NPCs forming neural rosettes in the heterozygous CUL3 KO cultures, whereas only Map-2 positive neurons were visible in all isogenic control cultures, as expected (Fig. 7A, B). Image analysis revealed a significantly higher density of neural rosettes in cultures from heterozygous CUL3 KO clones 6 and 19 compared to isogenic wildtypes (Fig. 8).

Cortical neurons differentiated from WT and CUL3 KO iPSC were also double immunostained for Map-2, and for vesicular glutamate transporter (vGlut-1), a marker for glutamatergic neurons. Consistent with published data (Shi Y et al., 2012), 88% – 93% of the Map-2 stained neurons were vGlut-1 positive glutamatergic neurons. High content image analysis did not detect significant differences between the genotypes. Finally, we analyzed the number of synaptic puncta labeled by the presynaptic marker, Synapsin 1/2 (Syn-1/2), and the postsynaptic marker, postsynaptic density protein 95 (Psd-95), which localize close to Map-2 positive dendrites. High content image analysis revealed a significant reduction in Syn-1/2 positive, presynaptic puncta per micrometer dendrite in cultures from heterozygous CUL3 KO clones 6 and 19 compared to isogenic wildtypes. (Fig. 9).

Heterozygous CUL3 KO neurons show decreased excitability following direct neuronal conversion from iPSCs

Several studies have demonstrated that lentiviral expression of the transcription factor Neurogenin-2 (NGN2) directly converts human iPSCs into a homogenous population of electrically-active, cortical glutamatergic neurons within 3 weeks (Nehme R et al., 2018; Zhang Y et al., 2013). NGN2-mediated direct neuronal conversion has already been used to analyze iPSC-models of various neuropsychiatric disorders (Pak C et al., 2015; Schafer ST et al., 2019; Zhang Y et al., 2013), and may be particularly useful for high throughput screening (Wang C et al., 2017). Moreover, CUL3 has been functionally annotated to non-coding, genetic risk variants for SZ by chromatin conformation capture assays using NGN2-induced neurons (Rajarajan P et al., 2018). Therefore, we transduced the heterozygous CUL3 KO iPSC lines and the isogenic control lines with a lentivirus encoding NGN2 in a second set of experiments. Eight days after lentivirus transduction, cells were dot-seeded onto 24-well glass-bottom, MEA plates. We started recording spontaneous electrical activity at div 14 after dot-seeding, when spontaneous firing becomes detectable in NGN2-induced neurons (Nehme R et al., 2018; Zhang Y et al., 2013). Spike rate steadily increased both in heterozygous CUL3 KO neuron cultures and in isogenic wildtype control cultures following direct neuronal conversion (Fig. 6B). By multi-parametric analysis of spontaneous spikes, bursts, and network bursts, we could not detect significant differences in NGN2-induced CUL3 KO versus WT neuron cultures (Fig. 6C).

By bright-field microscopy of the glass-bottom MEA plates, neural rosettes were not visible in CUL3 KO cultures and in controls. In parallel, iPSC lines were directly converted into glutamatergic neurons on 96-well cell culture plates. Following immunostaining for the RGC/NPC marker Pax-6 and the neuronal marker Map-2 at div 27, only Map-2 positive neurons were detectable both in heterozygous CUL3 KO cultures and in isogenic wildtype controls (Fig. 7C, D).

By qRT-PCR we could detect only negligible levels of SLC1A3 mRNA expression (mean C_T > 35.0) in cortical neurons following NGN2-mediated direct neuronal conversion from iPSCs, which is consistent with RNA-sequencing data published by others (Tian R et al., 2019), and confirms that RGCs/NPCs are absent (Zhang Y et al., 2013). However, we detected a robust expression of CUL3 transcripts in induced wildtype neurons, which significantly decreased by approximately 50% in induced CUL3 KO neurons.

To analyze evoked neuronal excitability, we transduced our iPSC lines with lentiviral NGN2 and a lentiviral vector encoding channelrhodopsin-2 (ChR2), which allows artifact-free, optogenetic stimulation of induced neurons on MEA plates (Clements IP et al., 2016). Exposure of ChR2 expressing neurons on MEA plates to ten brief blue light pulses (50 ms, 470 nm) elicited time-locked spikes, as shown by the raster plots in Fig. 10A. As expected, exposure of transduced neurons to red light (50 ms, 590 nm) or light exposure of non-transduced neurons did not elicit any neuronal response (not shown). More importantly, the increase in spike rate following optogenetic stimulation at increasing light intensity was significantly smaller in heterozygous CUL3 KO neuron cultures compared to isogenic WT control cultures (Fig. 10B). Furthermore, at the highest light intensity, evoked activity declined in CUL3 KO cultures after 5 light pulses (Fig. 10A). Electrical stimulation and calcium imaging on a fluorometric imaging plate reader (FLIPR Tetra) confirmed decreased excitability of NGN2-induced CUL3 KO neurons (Fig. 10C), thus showing that hypoexcitability does not depend on the stimulation paradigm or the read-out.

Analysis of RhoA, Notch, and FGF signaling in CUL3 KO NPCs

Finally, we tried to identify the protein substrates and signaling pathways, which may be affected by Cullin-3 deficiency, and which may underlie the maintenance of the RGC/NPC stage in heterozygous CUL3 KO cultures. In non-neuronal human HeLa cells, CUL3 knockdown by small hairpin RNA led to an impaired ubiquitination and degradation of the small GTPase RhoA (Chen Y et al., 2009). Moreover, network analysis implicated a Cullin-3/RhoA pathway in human brain development and psychiatric diseases (Lin GN et al., 2015). By immunoblot analysis we detected similar levels of RhoA protein in heterozygous CUL3 KO

iPSCs/NPCs and isogenic controls (Fig. 11A), speaking against a major contribution of altered RhoA signaling in our iPSC model.

During mammalian brain development, Notch receptor signaling is required to maintain NPCs in an undifferentiated, self-renewing state. Following ligand binding and receptor proteolysis, the Notch intracellular domain activates target genes of the HES/HEY families, which subsequently suppress the expression of proneuronal genes (reviewed in (Pierfelice T et al., 2011)). Conditional deletion of the Cullin-1 adaptor protein Fbxw7 leads to an accumulation of Notch protein and HES5/HEY1/HEY2 transcripts in the embryonic mouse brain, demonstrating that Notch signaling during mammalian neurodevelopment is controlled by Cullin ubiquitin ligases (Matsumoto A et al., 2011). By qRT-PCR we detected similar levels of HES5/HEY1 mRNA in heterozygous CUL3 KO NPCs and isogenic WT controls, giving indirect evidence that the maintenance of RGCs/NPCs in CUL3 KO cultures during small molecule-mediated neuronal differentiation is not caused by enhanced Notch signaling. It should be noted, that we cultured proliferating NPCs in the absence of the Notch inhibitor DAPT (see Experimental Procedures), and thus, an effect of Cullin-3 deficiency on endogenous Notch signaling should be detectable by changes in Notch target gene expression.

Fibroblast growth factors (FGFs) are crucial for maintenance of NPCs in the developing forebrain (reviewed in (Guillemot F and Zimmer C, 2011; Mason I, 2007)), and recombinant FGF2 was added to our NPC cultures to promote proliferation and self-renewal. FGF signaling is regulated by ubiquitylation and targeted degradation of the activated FGF receptor by the ubiquitin ligase Cbl. Downstream MAPK signaling is particularly important for the mitogenic activity of FGFs. The MAPK cascade triggers transcriptional activation of effectors (e.g. ETV1, CREB1) and feedback inhibitors (e.g. SPRY1, IL17RD/SEF) of FGF receptor signaling (reviewed in (Guillemot F and Zimmer C, 2011; Mason I, 2007)). Interestingly, we detected significantly decreased mRNA levels of the feedback inhibitors SPRY1 and IL17RD/SEF in heterozygous CUL3 KO NPCs, while mRNA levels of the effectors remained unchanged (Fig. 11B).

DISCUSSION

Cullin-3 is an E3 ubiquitin ligase that ubiquitylates numerous protein substrates by binding to diverse adaptor proteins (reviewed in (Petroski MD and Deshaies RJ, 2005)). Cullin-3 complexes catalyze both proteolytic and non-proteolytic ubiquitin signals, thereby regulating many fundamental biological processes, like cell division, embryonic development, DNA synthesis/repair, and cytoskeleton dynamics. Not surprisingly, loss-of-function mutations in CUL3 or its adaptor proteins are linked to severe human diseases, including metabolic

disorders, muscle/nerve degeneration, and cancer (reviewed in (Genschik P et al., 2013; Jerabkova K and Sumara I, 2018)). Moreover, the CUL3 gene is listed as one of the 23 top ranking, high confidence risk genes for autism spectrum disorder (ASD) in the SFARI Gene database (gene.safari.org/database). Rare, protein-truncating mutations in the CUL3 gene (e.g. p.Ser133X, p.Glu246X, p.Arg546X) were detected by independent sequencing studies in large cohorts of ASD families (da Silva Montenegro EM et al., 2019; Kong A et al., 2012; O'Roak BJ et al., 2012; Ruzzo EK et al., 2019). Unfortunately, clinical records of the mutation carriers were not reported. Large GWAS of schizophrenia have identified common, low risk genetic variants, most of them in intronic or intergenic regions of the human genome (Pardinas AF et al., 2018; Schizophrenia Working Group of the Psychiatric Genomics C, 2014). For functional annotation of these non-coding risk loci to causal genes, open chromatin profiling and chromosome interaction mapping were performed using both human brain tissue and iPSC-derived NPCs/neurons (Forrest MP et al., 2017; Li M et al., 2018; Rajarajan P et al., 2018). NPCs/neurons were derived from human iPSC using either small molecules or direct conversion, as in the present study. Notably, CUL3 was identified in chromosomal contacts anchored to SZ risk loci both in NPCs and in neurons (Rajarajan P et al., 2018; Song M et al., 2019), indicating that iPSC-derived human NPCs/neurons are well-suited to elucidate the (patho-)physiological function of Cullin-3. Whether these non-coding, gene-regulatory risk variants up- or down-regulate CUL3 gene expression, remains to be tested. Furthermore, analysis of gene coexpression modules identified CUL3 in a module (ME2) that is highly expressed in the prenatal human brain and enriched in RGCs/NPCs/neurons (Li M et al., 2018). These findings are consistent with prior network analyses of ASD risk genes including CUL3 (Lin GN et al., 2015; Willsey AJ et al., 2013), and suggest that these risk variants for ASD/SZ may disrupt neurodevelopmental processes.

The function of Cullin-3 in the nervous system has been investigated mainly in non-mammalian species. In Drosophila melanogaster, a splicing mutation in CUL3 caused a massive defect in neurite elongation of mushroom body neurons (Zhu S et al., 2005), and a genetic screen identified a role for Cullin-3 in presynaptic homeostatic potentiation in the neuromuscular junction (Kikuma K et al., 2019). In the nematode Caenorhabditis elegans, both an endogenous protein-truncating mutation in the Cullin-3 adaptor protein KEL-8 and transgenic overexpression of dominant negative Cullin-3 fragments resulted in decreased synaptic turnover of AMPA-type glutamate receptor subunits (Schaefer H and Rongo C, 2006). By contrast, levels of AMPA receptor subunits were unchanged in synaptosome preparations from heterozygous CUL3 knockout mouse brains, while kainate receptor subunits accumulated by about 20% (Salinas GD et al., 2006). Little is known about the function of Cullin-3 in human neurodevelopment. Knockdown of the Cullin-3 adaptor KBTBD8 by short hairpin RNA in

human embryonic stem cell cultures did not affect proliferation or pluripotency. Following small molecule-mediated neural differentiation however, knockdown of KBTBD8 resulted in an increase in CNS neuronal precursor cells and a decline in neural crest cells (Werner A et al., 2015).

Since fibroblasts from psychiatric patients carrying rare, protein-truncating mutations in the CUL3 gene were not available for reprogramming, we used CRISPR/Cas9 nickase to knockout CUL3 in human iPSCs from healthy donors. This approach generates isogenic iPSC lines, thereby minimizing genetic background heterogeneity (Jinek M et al., 2012; Kim HS et al., 2014), and reduces off-target effects observed with Cas9 nuclease (Ran FA et al., 2013). By DNA sequencing, we detected a 3 bp, in-frame deletion in iPSC clone 6, and a 17 bp deletion in clone 19. Consistent with CUL3 gene targeting in mice (Singer JD et al., 1999), we detected only heterozygous CUL3 KO iPSC lines. The 17 bp, frameshift deletion in clone 19 is predicted to lead to a premature stop codon (p.Phe199X), which may result in nonsense-mediated mRNA decay (Chang YF et al., 2007) of the mutant CUL3 transcript. By contrast, the decrease in CUL3 mRNA in clone 6 carrying a 3 bp in-frame deletion, is surprising. According to three-dimensional models of the protein structure of Cullin E3 ligases (Petroski MD and Deshaies RJ, 2005; Zheng N et al., 2002), the single amino acid (Glu202 or Glu203) deletion of clone 6 is located in an alpha-helix of the Cullin repeat motif. Moreover, amino acids Glu202 and Glu203 are highly conserved between species. The N-terminal Cullin repeats have a rigid structure, which is required to juxtapose the protein substrate and the E2 enzyme for ubiquitin transfer, since mutations that increase flexibility destroyed Cullin E3 activity (Petroski MD and Deshaies RJ, 2005; Zheng N et al., 2002). It may be hypothesized, that deletion of Glu202 or Glu203 has a deleterious effect on the structure/rigidity of the Cullin repeat, and consequently the stability/activity of Cullin-3 (Schumacher FR et al., 2015). Interestingly, similar findings have been published in the non-related protein Kindlin-1, where an in-frame deletion of a single amino acid in a highly structured region affected protein structure and led to a massive reduction of mRNA and protein (Maier K et al., 2016). By immunoblot analyses using two different anti-Cullin-3 antibodies, we detected an approximate 50% reduction in Cullin-3 protein levels in the two heterozygous CUL3 KO iPSC clones, and a Cullin-3 band migrating at a slightly higher molecular weight in CUL3 KO clone 19. It may be speculated that the reduction in Cullin-3 protein in heterozygous CUL3 KO iPSC leads to an increase in post-translational modifications (e.g. neddylation, autoubiquitylation) of Cullin-3 encoded by the wildtype allele (Genschik P et al., 2013; Petroski MD and Deshaies RJ, 2005). Alternatively, structural changes in the mutant Cullin-3 protein may increase neddylation and autoubiquitinylation as shown by others (Schumacher FR et al., 2015). It remains unclear however, why the shift in the Cullin-3 protein band is not detectable in the heterozygous CUL3 KO clone 6. An about

50% neddylation of Cullin-3 has been detected in mouse embryonic stem cells plated on gelatin using a different antibody (Jin L et al., 2012). Our immunoblot analyses suggest that the basal levels of neddylated Cullin-3 are lower in human iPSCs plated on Matrigel. In addition, differential splicing of CUL3, which has recently been demonstrated both in human NPC cultures and in the mouse forebrain (Burke EE et al., 2020; Furlanis E et al., 2019), might contribute to the shift of the Cullin-3 band in our immunoblot analysis.

Although CUL3 mRNA is expressed in human iPSCs ((van de Leemput J et al., 2014) and present study), our heterozygous KO of CUL3 by Cas9 nickase did not affect expression of various markers for pluripotency, which is consistent with unaltered expression of pluripotency markers in mouse embryonic stem cells depleted of CUL3 by short interfering RNA treatment (Jin L et al., 2012). Messenger RNA expression of CUL3 remains at high levels during small molecule-mediated neuronal differentiation of iPSC ((van de Leemput J et al., 2014) and present study). At the NPC stage, we detected a moderate increase in cell proliferation of the three CUL3 KO clones by EdU labeling during DNA replication, which is consistent with findings in embryonic fibroblasts from heterozygous CUL3 KO mice (McEvoy JD et al., 2007). To profile expression of genes regulating neuronal development and function, we used 96-well qPCR arrays. Bulk or single cell RNA-sequencing will be required however, to get a more complete picture of changes in gene expression and signaling pathways induced by Cullin-3 deficiency. Both by PCR Human Neurogenesis arrays and by qRT-PCR, we detected an approximate 3-fold increase in PAX6 mRNA levels in heterozygous CUL3 KO NPCs derived from clone 6 and clone 19. In the embryonic mouse cortex, PAX6 plays an essential role in the differentiation of radial glia cells (RGCs) (Gotz M et al., 1998), and in cultured mouse embryonic stem cells, PAX6 knockdown decreased differentiation of neuroepithelial cells to RGCs (Suter DM et al., 2009). Additionally, we found a moderate decrease in TENM1 mRNA expression. The protein product, teneurin-1, has a role in synapse organization and neurite elongation in mice (reviewed in (Mosca TJ, 2015)). By PCR Human Neurotransmitter array analysis and by qRT-PCR of 14 days old, iPSC-derived neurons, we found a > 3-fold increase in mRNA levels of the glutamate transporter, solute carrier family 1 member 3 (SLC1A3), in heterozygous CUL3 KO neurons derived from clone 6 and clone 19. SLC1A3 (EAAT1, GLAST1) is best known as the astrocytic glutamate transporter, which takes up the neurotransmitter glutamate after release from neuronal synapses (Hertz L and Zielke HR, 2004). In our iPSC-derived neuron cultures however, astrocytes become detectable only after 45 days of small molecule differentiation ((Shi Y et al., 2012) and present study). By single cell RNA sequencing of the developing human neocortex, independent studies demonstrated preferential expression of SLC1A3 in proliferating RGCs and NPCs (Johnson MB et al., 2015; Polioudakis D et al., 2019; Zhong S et al., 2018). Thus, higher mRNA levels of the RGC/NPC

markers PAX6 and SLC1A3 in our heterozygous CUL3 KO cultures may indicate that these cells are retained in the RGC/NPC stage during small molecule-mediated neuronal differentiation. Consistently, we observed an appearance of Pax-6 positive NPCs forming neural rosettes in CUL3 KO neuron cultures. These proliferating CUL3 KO RGCs/NPCs overgrow the neuron cultures, which resulted in a (seeming) decline in neuronal electrical activity during our MEA recordings. Higher levels of PAX6 mRNA expression and higher numbers of Pax6-positive RGCs/NPCs in heterozygous CUL3 KO clone 8 compared to KO clone 19 might be partially explained by lower levels of CUL3 protein expression and protein modification in clone 8. However, since genomic instability has been reported in several iPSC studies (reviewed in (Drakulic D et al., 2020)), we cannot formally exclude a contribution by small genomic alterations that escaped detection by our array-based karyotype analysis and that can only be ruled out by whole genome sequencing. It should be noted, that we did not add antimitotic agents, like cytosine arabinoside (Ara-C), to our cultures of iPSC-derived neurons. Ara-C has been added to the medium in other iPSC studies to inhibit proliferation of non-neuronal cells and cocultured astrocytes, but Ara-C may also prevent growth of persisting RGCs/NPCs during neuronal differentiation in iPSC models of neurodevelopmental disorders. Increased expression of marker genes for immature neurons, a decrease in spontaneous neuronal network activity over time, and impaired synaptic plasticity were also detected in iPSC-derived cortical neurons of patients diagnosed with ASD, Angelman syndrome, and childhood-onset schizophrenia, respectively (Fink JJ et al., 2017; Flaherty E et al., 2019; Marchetto MC et al., 2017). Taken together, there is increasing evidence that deficits in neuronal differentiation are a point of convergence in iPSC models of neurodevelopmental/neuropsychiatric disorders (reviewed in (Ahmad R et al., 2018; Ernst C, 2016; Ichida JK and Kiskinis E, 2015)). These neurodevelopmental deficits may be exacerbated (e.g. overgrowth of iPSC-derived neurons by persisting RGCs/NPCs in the present study) in iPSC models grown in two-dimensional culture on exogenous extracellular matrix, however, numerous neuropathological studies of postmortem cortical tissue from autistic children revealed signs of extended neurogenesis, neuronal immaturity, and abnormal migration consistent with dysregulation of neuronal differentiation at prenatal stages (Kaushik G and Zarbalis KS, 2016; Stoner R et al., 2014; Wegiel J et al., 2010).

Lentiviral expression of the neuralizing transcription factor NGN2 directly converts human iPSCs into cortical glutamatergic neurons and appears to circumvent the NPC stage (Zhang Y et al., 2013). By RNA sequencing robust CUL3 expression has been demonstrated at all time-points of direct neuronal conversion, while SLC1A3 expression could not be detected ((Tian R et al., 2019) and present study). Overexpression of NGN2 in RGCs of the developing ferret cortex shifts RGCs into postmitotic neurons (Johnson MB et al., 2015). These data might

explain, why the persistence of RGCs/NPCs in CUL3 KO cultures during small molecule-mediated neuronal differentiation was not observed during NGN2-mediated direct neuronal conversion in our study. Our findings also sound a note of caution. Risk genes for neurodevelopmental/neuropsychiatric disorders are significantly enriched in RGCs/NPCs of the prenatal human neocortex (Polioudakis D et al., 2019; Schork AJ et al., 2019), and non-coding risk variants have been identified in human-specific enhancers that regulate the proliferation of outer RGCs. This cell type is particularly important for the evolutionary expansion of the human neocortex and the increased cognitive abilities of humans (de la Torre-Ubieta L et al., 2018). Therefore, disease-relevant, early neurodevelopmental alterations induced by these risk genes in iPSC models may be obscured by direct neuronal conversion, which bypasses the RGC/NPC stage. Similar findings have recently been reported in iPSCs from idiopathic, macrocephalic ASD patients, where NGN2-mediated direct conversion attenuated ASD-associated accelerated neurite outgrowth observed during small molecule differentiation (Schafer ST et al., 2019).

However, non-coding common variants for SZ form contacts with the CUL3 gene in NGN2-induced neurons (Rajarajan P et al., 2018) indicating that (patho-)physiological neuronal functions of Cullin-3 can be identified in induced cortical glutamatergic neurons. Although our multiparametric analysis of MEA recordings did not reveal significant differences in spontaneous spikes, bursts, and networks bursts between induced CUL3 KO neurons and isogenic controls, both optogenetic stimulation combined with MEA recordings and electrical stimulation combined with calcium imaging demonstrated a significant decrease in neuronal excitability. The rapid decline in evoked activity in CUL3 KO neurons after 5 light pulses may indicate enhanced short-term synaptic depression and/or accelerated depletion of readily releasable synaptic vesicles in glutamatergic synapses. Consistently, normal basal synaptic transmission and altered short-term synaptic plasticity have been reported in cortical pyramidal neurons of various genetic mouse models of SZ/ASD (reviewed in (Crabtree GW and Gogos JA, 2014)). Very recently, decreased excitability and spine loss has also been detected in cortical pyramidal neurons of heterozygous mice with forebrain-specific CUL3 deletion (Rapanelli M et al., 2019). Thus, both human iPSC models and mutant mouse models exhibit deficits in cortical glutamatergic signaling, which may represent one of the earliest pathophysiological alteration in schizophrenia (Krystal JH et al., 2017).

Signaling via both the Notch receptor and the FGF receptor is crucial for maintenance of NPCs in an undifferentiated, self-renewing state (reviewed in (Guillemot F and Zimmer C, 2011; Mason I, 2007; Pierfelice T et al., 2011)). Since both signaling cascades are regulated by Cullin E3 ligases (Guillemot F and Zimmer C, 2011; Mason I, 2007; Matsumoto A et al., 2011), we investigated the expression of known target genes of Notch and FGF, respectively, in

proliferating NPC cultures. While Notch target gene expression was unaltered in heterozygous CUL3 KO NPCs, expression of feedback inhibitors of FGF signaling (SPRY1, IL17RD) was significantly reduced. Interestingly, human brain-specific gene network analysis identified FGF1 and FGFR2 as key intermediate genes linking high confidence ASD genes to disorder-related pathways (Krishnan A et al., 2016). Moreover, by gene expression profiling increased FGF2 mRNA expression was detected in the temporal cortex of autism patients (Garbett K et al., 2008). Although further studies are required to clarify whether Cullin-3 deficiency directly or indirectly affects FGF signaling, our study indicates that Cullin-3 ubiquitin ligase regulates differentiation of human cortical RGCs/NPCs, which might contribute to the neurodevelopmental deficits in psychiatric disorders associated with CUL3 loss-of-function mutations.

Acknowledgements

The authors thank Selina Reich for nucleofection of iPSCs, Dr. Stefan Jäger for help with digital image analysis, Dr. Bernd-Wolfgang Igl (all Boehringer Ingelheim Pharma GmbH & Co. KG, Biberach, Germany) for expert advice concerning statistical analysis, and Prof. Vania Broccoli (Ospedale San Raffaele, Milan, Italy) for providing lentiviral vectors.

Abbreviations

ASD, autism spectrum disorder; Cas9n, Cas9 nickase; GWAS, genome-wide association study; iPSC, induced pluripotent stem cell; NPC, neural precursor cell; qRT-PCR, quantitative real time PCR; RGC, radial glia cell; SZ, schizophrenia

REFERENCES

Ahmad R, Sportelli V, Ziller M, Spengler D, Hoffmann A (2018), Tracing Early Neurodevelopment in Schizophrenia with Induced Pluripotent Stem Cells. Cells 7.

Bahari-Javan S, Varbanov H, Halder R, Benito E, Kaurani L, Burkhardt S, Anderson-Schmidt H, Anghelescu I, et al. (2017), HDAC1 links early life stress to schizophrenia-like phenotypes. Proc Natl Acad Sci U S A 114:E4686-e4694.

Brennand K, Savas JN, Kim Y, Tran N, Simone A, Hashimoto-Torii K, Beaumont KG, Kim HJ, et al. (2015), Phenotypic differences in hiPSC NPCs derived from patients with schizophrenia. Mol Psychiatry 20:361-368.

Brennand KJ, Simone A, Jou J, Gelboin-Burkhart C, Tran N, Sangar S, Li Y, Mu Y, et al. (2011), Modelling schizophrenia using human induced pluripotent stem cells. Nature 473:221-225.

Burke EE, Chenoweth JG, Shin JH, Collado-Torres L, Kim SK, Micali N, Wang Y, Colantuoni C, et al. (2020), Dissecting transcriptomic signatures of neuronal differentiation and maturation using iPSCs. Nat Commun 11:462.

Chambers SM, Fasano CA, Papapetrou EP, Tomishima M, Sadelain M, Studer L (2009), Highly efficient neural conversion of human ES and iPS cells by dual inhibition of SMAD signaling. Nat Biotechnol 27:275-280.

Chang YF, Imam JS, Wilkinson MF (2007), The nonsense-mediated decay RNA surveillance pathway. Annu Rev Biochem 76:51-74.

Chen Y, Yang Z, Meng M, Zhao Y, Dong N, Yan H, Liu L, Ding M, et al. (2009), Cullin mediates degradation of RhoA through evolutionarily conserved BTB adaptors to control actin cytoskeleton structure and cell movement. Mol Cell 35:841-855.

Clements IP, Millard DC, Nicolini AM, Preyer AJ, Grier R, Heckerling A, Blum RA, Tyler P, et al. (2016) Optogenetic stimulation of multiwell MEA plates for neural and cardiac applications. SPIE.

Codina-Sola M, Rodriguez-Santiago B, Homs A, Santoyo J, Rigau M, Aznar-Lain G, Del Campo M, Gener B, et al. (2015), Integrated analysis of whole-exome sequencing and transcriptome profiling in males with autism spectrum disorders. Mol Autism 6:21.

Colasante G, Lignani G, Rubio A, Medrihan L, Yekhlef L, Sessa A, Massimino L, Giannelli SG, et al. (2015), Rapid Conversion of Fibroblasts into Functional Forebrain GABAergic Interneurons by Direct Genetic Reprogramming. Cell Stem Cell 17:719-734.

Crabtree GW, Gogos JA (2014), Synaptic plasticity, neural circuits, and the emerging role of altered short-term information processing in schizophrenia. Frontiers in synaptic neuroscience 6:28.

da Silva Montenegro EM, Costa CS, Campos G, Scliar M, de Almeida TF, Zachi EC, Silva IMW, Chan AJS, et al. (2019), Meta-Analyses Support Previous and Novel Autism Candidate Genes: Outcomes of an Unexplored Brazilian Cohort. Autism research : official journal of the International Society for Autism Research.

de la Torre-Ubieta L, Stein JL, Won H, Opland CK, Liang D, Lu D, Geschwind DH (2018), The Dynamic Landscape of Open Chromatin during Human Cortical Neurogenesis. Cell 172:289-304.e218.

Drakulic D, Djurovic S, Syed YA, Trattaro S, Caporale N, Falk A, Ofir R, Heine VM, et al. (2020), Copy number variants (CNVs): a powerful tool for iPSC-based modelling of ASD. Mol Autism 11:42.

916 Ernst C (2016), Proliferation and Differentiation Deficits are a Major Convergence Point for
917 Neurodevelopmental Disorders. Trends in neurosciences 39:290-299.
918 Fink JJ, Robinson TM, Germain ND, Sirois CL, Bolduc KA, Ward AJ, Rigo F, Chamberlain SJ, et al.
919 (2017), Disrupted neuronal maturation in Angelman syndrome-derived induced pluripotent
920 stem cells. Nat Commun 8:15038.
921 Flaherty E, Zhu S, Barretto N, Cheng E, Deans PJM, Fernando MB, Schrode N, Francoeur N, et
922 al. (2019), Neuronal impact of patient-specific aberrant NRXN1alpha splicing. Nat Genet
923 51:1679-1690.
924 Forrest MP, Zhang H, Moy W, McGowan H, Leites C, Dionisio LE, Xu Z, Shi J, et al. (2017), Open
925 Chromatin Profiling in hiPSC-Derived Neurons Prioritizes Functional Noncoding Psychiatric
926 Risk Variants and Highlights Neurodevelopmental Loci. Cell Stem Cell 21:305-318 e308.
927 Forrest MP, Zhang H, Moy W, McGowan H, Leites C, Dionisio LE, Xu Z, Shi J, et al. (2017), Open
928 Chromatin Profiling in hiPSC-Derived Neurons Prioritizes Functional Noncoding Psychiatric
929 Risk Variants and Highlights Neurodevelopmental Loci. Cell Stem Cell 21:305-318.e308.
930 Furlanis E, Traunmuller L, Fucile G, Scheiffele P (2019), Landscape of ribosome-engaged
931 transcript isoforms reveals extensive neuronal-cell-class-specific alternative splicing programs.
932 Nature neuroscience 22:1709-1717.
933 Garbett K, Ebert PJ, Mitchell A, Lintas C, Manzi B, Mirnics K, Persico AM (2008), Immune
934 transcriptome alterations in the temporal cortex of subjects with autism. Neurobiology of
935 disease 30:303-311.
936 Genschik P, Sumara I, Lechner E (2013), The emerging family of CULLIN3-RING ubiquitin ligases
937 (CRL3s): cellular functions and disease implications. Embo j 32:2307-2320.
938 Gotz M, Stoykova A, Gruss P (1998), Pax6 controls radial glia differentiation in the cerebral
939 cortex. Neuron 21:1031-1044.
940 Guillemot F, Zimmer C (2011), From cradle to grave: the multiple roles of fibroblast growth
941 factors in neural development. Neuron 71:574-588.
942 Hershko A, Ciechanover A (1998), The ubiquitin system. Annu Rev Biochem 67:425-479.
943 Hertz L, Zielke HR (2004), Astrocytic control of glutamatergic activity: astrocytes as stars of the
944 show. Trends in neurosciences 27:735-743.
945 Ichida JK, Kiskinis E (2015), Probing disorders of the nervous system using reprogramming
946 approaches. Embo j 34:1456-1477.
947 Jerabkova K, Sumara I (2018), Cullin 3, a cellular scripter of the non-proteolytic ubiquitin code.
948 Seminars in cell & developmental biology.
949 Jin L, Pahuja KB, Wickliffe KE, Gorur A, Baumgartel C, Schekman R, Rape M (2012), Ubiquitin-
950 dependent regulation of COPII coat size and function. Nature 482:495-500.
951 Jinek M, Chylinski K, Fonfara I, Hauer M, Doudna JA, Charpentier E (2012), A programmable
952 dual-RNA-guided DNA endonuclease in adaptive bacterial immunity. Science 337:816-821.
953 Johnson MB, Wang PP, Atabay KD, Murphy EA, Doan RN, Hecht JL, Walsh CA (2015), Single-
954 cell analysis reveals transcriptional heterogeneity of neural progenitors in human cortex.
955 Nature neuroscience 18:637-646.
956 Kang HJ, Kawasawa YI, Cheng F, Zhu Y, Xu X, Li M, Sousa AM, Pletikos M, et al. (2011), Spatio-
957 temporal transcriptome of the human brain. Nature 478:483-489.
958 Kaushik G, Zarbalis KS (2016), Prenatal Neurogenesis in Autism Spectrum Disorders. Frontiers
959 in chemistry 4:12.

960 Kikuma K, Li X, Perry S, Li Q, Goel P, Chen C, Kim D, Stavropoulos N, et al. (2019), Cul3 and
961 insomniac are required for rapid ubiquitination of postsynaptic targets and retrograde
962 homeostatic signaling. Nat Commun 10:2998.
963 Kim HS, Bernitz JM, Lee DF, Lemischka IR (2014), Genomic editing tools to model human
964 diseases with isogenic pluripotent stem cells. Stem Cells Dev 23:2673-2686.
965 Kizner V, Naujock M, Fischer S, Jager S, Reich S, Schlotthauer I, Zuckschwerdt K, Geiger T, et
966 al. (2019), CRISPR/Cas9-mediated Knockout of the Neuropsychiatric Risk Gene KCTD13 Causes
967 Developmental Deficits in Human Cortical Neurons Derived from Induced Pluripotent Stem
968 Cells. Mol Neurobiol.
969 Kizner V, Naujock M, Fischer S, Jäger S, Reich S, Schlotthauer I, Zuckschwerdt K, Geiger T, et
970 al. (2019), CRISPR/Cas9-mediated Knockout of the Neuropsychiatric Risk Gene KCTD13 Causes
971 Developmental Deficits in Human Cortical Neurons Derived from Induced Pluripotent Stem
972 Cells. Mol Neurobiol.
973 Kong A, Frigge ML, Masson G, Besenbacher S, Sulem P, Magnusson G, Gudjonsson SA,
974 Sigurdsson A, et al. (2012), Rate of de novo mutations and the importance of father's age to
975 disease risk. Nature 488:471-475.
976 Krishnan A, Zhang R, Yao V, Theesfeld CL, Wong AK, Tadych A, Volfovsky N, Packer A, et al.
977 (2016), Genome-wide prediction and functional characterization of the genetic basis of autism
978 spectrum disorder. Nature neuroscience 19:1454-1462.
979 Krystal JH, Anticevic A, Yang GJ, Dragoi G, Driesen NR, Wang XJ, Murray JD (2017), Impaired
980 Tuning of Neural Ensembles and the Pathophysiology of Schizophrenia: A Translational and
981 Computational Neuroscience Perspective. Biol Psychiatry 81:874-885.
982 Kyttala A, Moraghebi R, Valensisi C, Kettunen J, Andrus C, Pasumarthy KK, Nakanishi M,
983 Nishimura K, et al. (2016), Genetic Variability Overrides the Impact of Parental Cell Type and
984 Determines iPSC Differentiation Potential. Stem Cell Reports 6:200-212.
985 Lek M, Karczewski KJ, Minikel EV, Samocha KE, Banks E, Fennell T, O'Donnell-Luria AH, Ware
986 JS, et al. (2016), Analysis of protein-coding genetic variation in 60,706 humans. Nature
987 536:285-291.
988 Lewis DA, Gonzalez-Burgos G (2006), Pathophysiologically based treatment interventions in
989 schizophrenia. Nat Med 12:1016-1022.
990 Li M, Santpere G, Imamura Kawasawa Y, Evgrafov OV, Gulden FO, Pochareddy S, Sunkin SM,
991 Li Z, et al. (2018), Integrative functional genomic analysis of human brain development and
992 neuropsychiatric risks. Science 362.
993 Lin GN, Corominas R, Lemmens I, Yang X, Tavernier J, Hill DE, Vidal M, Sebat J, et al. (2015),
994 Spatiotemporal 16p11.2 protein network implicates cortical late mid-fetal brain development
995 and KCTD13-Cul3-RhoA pathway in psychiatric diseases. Neuron 85:742-754.
996 Maier K, He Y, Esser PR, Thriene K, Sarca D, Kohlhase J, Dengjel J, Martin L, et al. (2016), Single
997 Amino Acid Deletion in Kindlin-1 Results in Partial Protein Degradation Which Can Be Rescued
998 by Chaperone Treatment. The Journal of investigative dermatology 136:920-929.
999 Marchetto MC, Belinson H, Tian Y, Freitas BC, Fu C, Vadodaria K, Beltrao-Braga P, Trujillo CA,
1000 et al. (2017), Altered proliferation and networks in neural cells derived from idiopathic autistic
1001 individuals. Mol Psychiatry 22:820-835.
1002 Marchetto MC, Carromeu C, Acab A, Yu D, Yeo GW, Mu Y, Chen G, Gage FH, et al. (2010), A
1003 model for neural development and treatment of Rett syndrome using human induced
1004 pluripotent stem cells. Cell 143:527-539.

Mason I (2007), Initiation to end point: the multiple roles of fibroblast growth factors in neural development. Nat Rev Neurosci 8:583-596.
Matsumoto A, Onoyama I, Sunabori T, Kageyama R, Okano H, Nakayama KI (2011), Fbxw7-dependent degradation of Notch is required for control of "stemness" and neuronal-glial differentiation in neural stem cells. J Biol Chem 286:13754-13764.
McEvoy JD, Kossatz U, Malek N, Singer JD (2007), Constitutive turnover of cyclin E by Cul3 maintains quiescence. Mol Cell Biol 27:3651-3666.
Millan MJ, Andrieux A, Bartzokis G, Cadenhead K, Dazzan P, Fusar-Poli P, Gallinat J, Giedd J, et al. (2016), Altering the course of schizophrenia: progress and perspectives. Nat Rev Drug Discov 15:485-515.
Morrison M, Klein C, Clemann N, Collier DA, Hardy J, Heisserer B, Cader MZ, Graf M, et al. (2015), StemBANCC: Governing Access to Material and Data in a Large Stem Cell Research Consortium. Stem Cell Rev 11:681-687.
Mosca TJ (2015), On the Teneurin track: a new synaptic organization molecule emerges. Front Cell Neurosci 9:204.
Murai K, Sun G, Ye P, Tian E, Yang S, Cui Q, Sun G, Trinh D, et al. (2016), The TLX-miR-219 cascade regulates neural stem cell proliferation in neurodevelopment and schizophrenia iPSC model. Nat Commun 7:10965.
Nehme R, Zuccaro E, Ghosh SD, Li C, Sherwood JL, Pietilainen O, Barrett LE, Limone F, et al. (2018), Combining NGN2 Programming with Developmental Patterning Generates Human Excitatory Neurons with NMDAR-Mediated Synaptic Transmission. Cell Rep 23:2509-2523.
O'Roak BJ, Vives L, Girirajan S, Karakoc E, Krumm N, Coe BP, Levy R, Ko A, et al. (2012), Sporadic autism exomes reveal a highly interconnected protein network of de novo mutations. Nature 485:246-250.
Pak C, Danko T, Zhang Y, Aoto J, Anderson G, Maxeiner S, Yi F, Wernig M, et al. (2015), Human Neuropsychiatric Disease Modeling using Conditional Deletion Reveals Synaptic Transmission Defects Caused by Heterozygous Mutations in NRXN1. Cell Stem Cell 17:316-328.
Pardinas AF, Holmans P, Pocklington AJ, Escott-Price V, Ripke S, Carrera N, Legge SE, Bishop S, et al. (2018), Common schizophrenia alleles are enriched in mutation-intolerant genes and in regions under strong background selection. Nat Genet 50:381-389.
Pasca SP, Portmann T, Voineagu I, Yazawa M, Shcheglovitov A, Pasca AM, Cord B, Palmer TD, et al. (2011), Using iPSC-derived neurons to uncover cellular phenotypes associated with Timothy syndrome. Nat Med 17:1657-1662.
Petroski MD, Deshaies RJ (2005), Function and regulation of cullin-RING ubiquitin ligases. Nat Rev Mol Cell Biol 6:9-20.
Pierfelice T, Alberi L, Gaiano N (2011), Notch in the vertebrate nervous system: an old dog with new tricks. Neuron 69:840-855.
Polioudakis D, de la Torre-Ubieta L, Langerman J, Elkins AG, Shi X, Stein JL, Vuong CK, Nichterwitz S, et al. (2019), A Single-Cell Transcriptomic Atlas of Human Neocortical Development during Mid-gestation. Neuron 103:785-801.e788.
Qi Y, Zhang XJ, Renier N, Wu Z, Atkin T, Sun Z, Ozair MZ, Tchieu J, et al. (2017), Combined small-molecule inhibition accelerates the derivation of functional cortical neurons from human pluripotent stem cells. Nat Biotechnol 35:154-163.
Rajarajan P, Borrman T, Liao W, Schrode N, Flaherty E, Casiño C, Powell S, Yashaswini C, et al. (2018), Neuron-specific signatures in the chromosomal connectome associated with schizophrenia risk. Science 362:eaat4311.

Ran FA, Hsu PD, Lin CY, Gootenberg JS, Konermann S, Trevino AE, Scott DA, Inoue A, et al. (2013), Double nicking by RNA-guided CRISPR Cas9 for enhanced genome editing specificity. Cell 154:1380-1389.

Rapanelli M, Tan T, Wang W, Wang X, Wang ZJ, Zhong P, Frick L, Qin L, et al. (2019), Behavioral, circuitry, and molecular aberrations by region-specific deficiency of the high-risk autism gene Cul3. Mol Psychiatry.

Ruzzo EK, Perez-Cano L, Jung JY, Wang LK, Kashef-Haghighi D, Hartl C, Singh C, Xu J, et al. (2019), Inherited and De Novo Genetic Risk for Autism Impacts Shared Networks. Cell 178:850-866.e826.

Salinas GD, Blair LA, Needleman LA, Gonzales JD, Chen Y, Li M, Singer JD, Marshall J (2006), Actinfilin is a Cul3 substrate adaptor, linking GluR6 kainate receptor subunits to the ubiquitin-proteasome pathway. J Biol Chem 281:40164-40173.

Schaefer H, Rongo C (2006), KEL-8 is a substrate receptor for CUL3-dependent ubiquitin ligase that regulates synaptic glutamate receptor turnover. Molecular biology of the cell 17:1250-1260.

Schafer ST, Paquola ACM, Stern S, Gosselin D, Ku M, Pena M, Kuret TJM, Liyanage M, et al. (2019), Pathological priming causes developmental gene network heterochronicity in autistic subject-derived neurons. Nature neuroscience 22:243-255.

Schizophrenia Working Group of the Psychiatric Genomics C (2014), Biological insights from 108 schizophrenia-associated genetic loci. Nature 511:421-427.

Schork AJ, Won H, Appadurai V, Nudel R, Gandal M, Delaneau O, Revsbech Christiansen M, Hougaard DM, et al. (2019), A genome-wide association study of shared risk across psychiatric disorders implicates gene regulation during fetal neurodevelopment. Nature neuroscience 22:353-361.

Schumacher FR, Siew K, Zhang J, Johnson C, Wood N, Cleary SE, Al Maskari RS, Ferryman JT, et al. (2015), Characterisation of the Cullin-3 mutation that causes a severe form of familial hypertension and hyperkalaemia. EMBO Mol Med 7:1285-1306.

Sheridan SD, Theriault KM, Reis SA, Zhou F, Madison JM, Daheron L, Loring JF, Haggarty SJ (2011), Epigenetic characterization of the FMR1 gene and aberrant neurodevelopment in human induced pluripotent stem cell models of fragile X syndrome. PLoS One 6:e26203.

Shi Y, Kirwan P, Livesey FJ (2012), Directed differentiation of human pluripotent stem cells to cerebral cortex neurons and neural networks. Nature protocols 7:1836-1846.

Shi Y, Kirwan P, Smith J, Robinson HP, Livesey FJ (2012), Human cerebral cortex development from pluripotent stem cells to functional excitatory synapses. Nat Neurosci 15:477-486, S471.

Singer JD, Gurian-West M, Clurman B, Roberts JM (1999), Cullin-3 targets cyclin E for ubiquitination and controls S phase in mammalian cells. Genes & development 13:2375-2387.

Song M, Yang X, Ren X, Maliskova L, Li B, Jones IR, Wang C, Jacob F, et al. (2019), Mapping cis-regulatory chromatin contacts in neural cells links neuropsychiatric disorder risk variants to target genes. Nat Genet 51:1252-1262.

Stoner R, Chow ML, Boyle MP, Sunkin SM, Mouton PR, Roy S, Wynshaw-Boris A, Colamarino SA, et al. (2014), Patches of disorganization in the neocortex of children with autism. N Engl J Med 370:1209-1219.

Sullivan PF, Kendler KS, Neale MC (2003), Schizophrenia as a complex trait: evidence from a meta-analysis of twin studies. Arch Gen Psychiatry 60:1187-1192.

Suter DM, Tirefort D, Julien S, Krause KH (2009), A Sox1 to Pax6 switch drives neuroectoderm to radial glia progression during differentiation of mouse embryonic stem cells. Stem cells (Dayton, Ohio) 27:49-58.

Tian R, Gachechiladze MA, Ludwig CH, Laurie MT, Hong JY, Nathaniel D, Prabhu AV, Fernandopulle MS, et al. (2019), CRISPR Interference-Based Platform for Multimodal Genetic Screens in Human iPSC-Derived Neurons. Neuron.

Tian R, Gachechiladze MA, Ludwig CH, Laurie MT, Hong JY, Nathaniel D, Prabhu AV, Fernandopulle MS, et al. (2019), CRISPR-based platform for multimodal genetic screens in human iPSC-derived neurons. bioRxiv:513309.

van de Leemput J, Boles NC, Kiehl TR, Corneo B, Lederman P, Menon V, Lee C, Martinez RA, et al. (2014), CORTECON: a temporal transcriptome analysis of in vitro human cerebral cortex development from human embryonic stem cells. Neuron 83:51-68.

Walsh T, McClellan JM, McCarthy SE, Addington AM, Pierce SB, Cooper GM, Nord AS, Kusenda M, et al. (2008), Rare structural variants disrupt multiple genes in neurodevelopmental pathways in schizophrenia. Science 320:539-543.

Wang C, Ward ME, Chen R, Liu K, Tracy TE, Chen X, Xie M, Sohn PD, et al. (2017), Scalable Production of iPSC-Derived Human Neurons to Identify Tau-Lowering Compounds by High-Content Screening. Stem Cell Reports 9:1221-1233.

Waterhouse A, Bertoni M, Bienert S, Studer G, Tauriello G, Gumienny R, Heer FT, de Beer TAP, et al. (2018), SWISS-MODEL: homology modelling of protein structures and complexes. Nucleic acids research 46:W296-w303.

Wegiel J, Kuchna I, Nowicki K, Imaki H, Wegiel J, Marchi E, Ma SY, Chauhan A, et al. (2010), The neuropathology of autism: defects of neurogenesis and neuronal migration, and dysplastic changes. Acta neuropathologica 119:755-770.

Werner A, Iwasaki S, McGourty CA, Medina-Ruiz S, Teerikorpi N, Fedrigo I, Ingolia NT, Rape M (2015), Cell-fate determination by ubiquitin-dependent regulation of translation. Nature 525:523-527.

Willsey AJ, Sanders SJ, Li M, Dong S, Tebbenkamp AT, Muhle RA, Reilly SK, Lin L, et al. (2013), Coexpression networks implicate human midfetal deep cortical projection neurons in the pathogenesis of autism. Cell 155:997-1007.

Zhang Y, Pak C, Han Y, Ahlenius H, Zhang Z, Chanda S, Marro S, Patzke C, et al. (2013), Rapid single-step induction of functional neurons from human pluripotent stem cells. Neuron 78:785-798.

Zheng N, Schulman BA, Song L, Miller JJ, Jeffrey PD, Wang P, Chu C, Koepp DM, et al. (2002), Structure of the Cul1-Rbx1-Skp1-F boxSkp2 SCF ubiquitin ligase complex. Nature 416:703-709.

Zhong S, Zhang S, Fan X, Wu Q, Yan L, Dong J, Zhang H, Li L, et al. (2018), A single-cell RNA-seq survey of the developmental landscape of the human prefrontal cortex. Nature 555:524-528.

Zhu S, Perez R, Pan M, Lee T (2005), Requirement of Cul3 for axonal arborization and dendritic elaboration in Drosophila mushroom body neurons. J Neurosci 25:4189-4197.

Figure Legends

Fig. 1. CRISPR/Cas9 nickase mediated CUL3 knockout in human induced pluripotent stem cells. (A) Identification of CRISPR/Cas9 nickase induced insertions/deletions in the CUL3 gene by T7 endonuclease cleavage assay. M, DNA marker; +/+_4, wildtype, parental control iPSC line CB4; +/+_2 and +/+_13, Cas9/gRNA-transfected, non-edited, wildtype iPSC clones 2 and 13, respectively; +/-_6 and +/-_19, Cas9/gRNA-transfected, heterozygous CUL3 knockout (KO) clones 6 and 19, respectively. (B) Quantitative RT-PCR analysis shows significantly decreased CUL3 mRNA expression in heterozygous CUL3 KO iPSC clones 6 and 19 (black boxes) compared to isogenic wildtype iPSC clones. Data from two independent experiments and three iPSC cultures per clone are shown in box-and whiskers plots. The box depicts the median and the 25th and 75th quartiles, and the whiskers show the 5th and 95th percentile. **p ≤ 0.01, ***p ≤ 0.001, unpaired Welch's t-tests. Additional information on statistical analysis is given in Supplementary Table S2. (C) DNA sequencing reveals an in-frame, 3 base pair deletion in heterozygous CUL3 KO iPSC clone 6 (+/-_6), and a 17 base pair deletion in heterozygous CUL3 KO iPSC clone 19 (+/-_19).

Fig. 2. Immunoblot analysis of Cullin-3 protein levels in iPSC lysates. (A) Representative immunoblots showing a decrease in Cullin-3 protein (black arrow) in heterozygous CUL3 KO iPSC, and a shift in the Cullin-3 band towards a higher molecular weight in heterozygous CUL3 KO clone 19. M, protein markers (colorimetric detection); +/+_4, wildtype, parental control iPSC line CB4; +/+_2 and +/+_13, Cas9/gRNA-transfected, non-edited, wildtype iPSC clones 2 and 13, respectively; +/-_6 and +/-_19, Cas9/gRNA-transfected, heterozygous CUL3 knockout (KO) clones 6 and 19, respectively. Both a monoclonal anti-Cullin-3 antibody raised against the N-terminus of human Cullin-3 (upper panel) and a polyclonal anti-Cullin-3 antibody raised against the C-terminus of human Cullin-3 were used for chemiluminescence detection. Immunoblot analysis of beta-Actin (lower panel) and reversible total protein staining of the membrane (panel on the right) confirm similar protein loading. (B) Densitometric analysis of all immunoblots shows a significant decrease in Cullin-3 protein levels in heterozygous CUL3 KO iPSC lines (black boxes) compared to isogenic WT control lines. Data from four independent experiments are shown in box-and whiskers plots. The box depicts the median and the 25th and 75th quartiles, and the whiskers show the 5th and 95th percentile. *p ≤ 0.05, **p ≤ 0.01, unpaired Welch's t-tests. Additional information on statistical analysis is given in Supplementary Table S2.

Fig. 3. CUL3 deficiency does not affect stemness of iPSC lines. Representative microscopic images of immunostainings for stemness markers Oct-4 and Tra-1-60 in iPSC cultures. Nuclei were stained with Hoechst 33342 and confocal images were analyzed using an Opera Phenix high-content image analysis system. Scale bars represent 100 µm. Data are given in the Results section.

Fig. 4. Effect of CUL3 deficiency on cell proliferation. (A) Representative example of digital image analysis of EdU-positive nuclei (green) in iPSC cultures. Nuclei were also stained with Hoechst 33342 dye (blue). Segmentation of the original microscopic image by Columbus software is shown from left to right (all nuclei, valid nuclei, EdU-positive and valid nuclei). (B) A trend towards increased proliferation is visible in heterozygous CUL3 KO (+/-) iPSC cultures compared to isogenic wildtype (+/+) control cultures (left histogram). A significant increase in proliferation is detectable in heterozygous CUL3 KO (+/-) NPC cultures (right histogram). $t(13.61) = 3.99$, $^{**}p \leq 0.01$, unpaired Welch's t-test. Data from 3-4 cultures per clone are shown in box-and whiskers plots. The box depicts the median and the 25th and 75th quartiles, and the whiskers show the 5th and 95th percentile. Scale bar represents 100 µm.

Fig. 5. (A) Histograms showing increased mRNA expression of the NPC marker PAX6 in NPC cultures of heterozygous CUL3 KO clones 6 and 19 (black bars), as detected by PCR array analysis (left panel) and qRT-PCR (right panel), respectively. $^{**}p \leq 0.01$, $^{***}p \leq 0.001$, unpaired Welch's t-tests. (B) Histograms showing increased mRNA expression of SLC1A3, a marker for radial glia cells and NPCs, in iPSC-derived neuron cultures from heterozygous CUL3 KO clones 6 and 19 (black bars), as detected by PCR array analysis (left panel) and qRT-PCR (right panel), respectively. $^{**}p \leq 0.01$, $^{****}p \leq 0.0001$, unpaired Welch's t-tests. (C) Immunostaining of NPC cultures and digital image analysis reveal significantly increased numbers of strongly Pax-6 immunofluorescent cells (green) in heterozygous CUL3 KO clones 6 and 19, whereas Nestin immunofluorescence (red) is unchanged. $^{**}p \leq 0.01$, unpaired Welch's t-tests. Quantitative RT-PCR and image analyses were performed using three cultures per clone. Histograms show mean ± SEM, and data points superimposed on the bars. Additional information on statistical analysis is given in Supplementary Table S2.

Fig. 6. Analysis of spontaneous electrical activity of iPSC-derived neurons using multi-electrode array (MEA) recordings. Human iPSC-derived neurons were dot-seeded onto 24-well, glass-bottom MEA plates following differentiation into cortical glutamatergic neurons either by small molecules (A) or by lentiviral NGN2 expression (B, C). (A) Wildtype iPSC-

derived neurons did not show a significant change in spontaneous activity from div 12 to div 23 after seeding, whereas heterozygous CUL3 KO clones 6 and 19 show a significant decrease in activity over time. ****p ≤ 0.0001, unpaired Welch's t-tests. The inset shows two neural rosettes (encircled) near an electrode (black) detected by bright field microscopy of the MEA plate. (B) Following NGN2-mediated direct neuronal conversion from iPSC, both wildtype iPSC-derived neurons and heterozygous CUL3 KO neurons exhibit a steady increase in spontaneous electrical activity during neuronal maturation. Data are shown in box-and whiskers plots. The box depicts the median and the 25th and 75th quartiles, and the whiskers show the 5th and 95th percentile. Detailed data analysis of (B) is shown in (C). (C) Multi-parametric analysis of spontaneous spikes, bursts, and network bursts during MEA recordings of induced wildtype neurons (from iPSC clones CB4, 2, and 13) and induced heterozygous CUL3 KO neurons (from clones 6 and 19) at various time-points (div 14, div 20, and div 27) after seeding onto MEA plates. a: spike rate (Hz); b: burst count; c: mean burst duration (s); d: mean burst spike count; e: mean burst spike rate (10Hz); f: spikes in bursts (%); g: mean interburst interval (s); h: spikes in network bursts (%). All parameters analyzed did not significantly differ between heterozygous CUL3 KO and wildtype neuron cultures following direct neuronal conversion from iPSC. Data from two independent MEA experiments, each comprising three cultures per clone. Additional information on statistical analysis is given in Supplementary Table S2.

Fig. 7. Immuofluorescent stainings for the neuron marker Map-2 (white) and the NPC marker Pax-6 (green) in neuron cultures derived from iPSCs. Human iPSCs were differentiated into cortical glutamatergic neurons using either small molecules (A, B), or lentiviral overexpression of Neurogenin-2 (NGN2) (C, D). Representative microscopic images show large clusters (neural rosettes) of Pax-6 positive NPCs in heterozygous CUL3 KO neuron cultures from clone 6 following small molecule-mediated neuronal differentiation (A), but not following NGN2-mediated direct neuronal conversion (C). Exclusively Map-2 positive neurons are visible in wildtype control cultures from clone CB4, as expected (B, D). Scale bars represent 100 µm. Overview images and quantitative analysis are shown in Fig. 8.

Fig. 8. Immuofluorescent stainings for the neuron marker Map-2 (red) and nuclear labeling using Hoechst 33342 dye (blue). Human iPSCs were differentiated into cortical glutamatergic neurons using small molecules. Representative composite microscopic images from Opera Phenix imaging system show numerous radial-symmetric neural rosettes in heterozygous CUL3 KO neuron cultures from clones 6 and 19. Exclusively Map-2 positive neurons are visible in wildtype control cultures. Scale bar represents 100 µm. Quantitative analysis of the number

of neural rosettes per region of interest (ROI) is shown in the box-and whiskers plot. The box depicts the median and the 25th and 75th quartiles, and the whiskers show the 5th and 95th percentile. ****p ≤ 0.0001, Kruskal Wallis test followed by pairwise Mann-Whitney U tests. Five ROIs per well and 10 wells per clone were analyzed. Additional information on statistical analysis is given in Supplementary Table S2.

Fig. 9. High-content image analyis of synaptic puncta labeled by the presynaptic marker, synapsin 1/2 (Syn-1/2), and the postsynaptic marker, postsynaptic density protein 95 (Psd-95), which are located close to Map-2 positive dendrites. (A, upper row) Detection of Map-2 immunoreactive (red) valid dendrites, and Syn-1/2 immunopositive (green) presynaptic puncta by Columbus software. (A, lower row) Representative microscopic images showing Psd-95 (green, left), vGlut-1 (green, right), and Map-2 (red) immunofluorescent signals. Scale bars represent 50 µm. (B) A significant reduction in Syn-1/2 positive, presynaptic puncta per micrometer neurite is detected in cultures from heterozygous CUL3 KO clones 6 and 19 compared to isogenic wildtypes. ****p ≤ 0.0001, unpaired Welch's t-tests. (C) The density of Psd-95 positive, postsynaptic puncta does not significantly differ between genotypes. 90-130 regions of interest per well, and 4 wells per clone were analyzed. Data are shown in box-and whiskers plots. The box depicts the median and the 25th and 75th quartiles, and the whiskers show the 5th and 95th percentile. Additional information on statistical analysis is given in Supplementary Table S2.

Fig. 10. Analysis of evoked electrical activity of NGN2-induced neurons using MEA recordings and calcium imaging, respectively. (A) Exposure of channelrhodopsin-2 expressing, induced neurons on MEA plates to ten blue light pulses evokes time-locked electrical spikes as shown by representative raster plots from isogenic wildtype clone CB4 and heterozygous CUL3 KO clone 6, respectively. The blue lines indicate light ON. At the highest light intensity (5 mA) evoked activity in CUL3 KO neuron cultures declines after 5 light pulses. (B) The increase in spike rate following optogenetic stimulation is significantly smaller in heterozygous CUL3 KO neuron cultures from clones 6 and 19 compared to isogenic WT control clones. **p ≤ 0.01, ***p ≤ 0.001, unpaired Welch's t-tests. (C) Electrical stimulation and calcium imaging of NGN2-induced neurons using a fluorometric imaging plate reader provides consistent results. A significant decrease in excitability of heterozygous CUL3 KO neurons from clones 6 and 19 is visible at increasing stimulus intensity, when compared to isogenic control clones. ***p ≤ 0.001, unpaired Welch's t-tests. Data are from 4-6 cultures per clone. Graphs depict mean ± SEM. Additional information on statistical analysis is given in Supplementary Table S2.

Fig. 11. (A, upper panel) Representative immunoblots showing similar levels of the putative Cullin-3 substrate RhoA in heterozygous CUL3 KO iPSCs and NPCs, respectively, compared to isogenic WT control cultures. (A, lower panel) Total protein stain confirms similar protein loading. M, protein markers (colorimetric detection); +/+_4, wildtype, parental control iPSC line CB4; +/+_2 and +/+_13, Cas9/gRNA-transfected, non-edited, wildtype iPSC clones 2 and 13, respectively; +/-_6 and +/-_19, Cas9/gRNA-transfected, heterozygous CUL3 knockout (KO) clones 6 and 19, respectively. (B) Analysis of target gene expression of FGFR/MAPK signaling in NPC cultures. Messenger RNA levels of the feedback inhibitors SPRY1 and IL17RD/SEF are significantly lower in heterozygous CUL3 KO NPCs. **p ≤ 0.01, unpaired Welch's t-tests. Data from 5-8 NPC cultures per clone are shown in box-and whiskers plots. The box depicts the median and the 25th and 75th quartiles, and the whiskers show the 5th and 95th percentile. Additional information on statistical analysis is given in Supplementary Table S2.

Highlights

- Heterozygous CUL3 knockout (ko) iPSC and isogenic control lines were generated using CRISPR/Cas9 nickase
- Neuronal differentiation by small molecules showed delayed transition from radial glia to neurons in CUL3 ko cultures
- Direct neuronal conversion of CUL3 ko iPSC by lentiviral Ngn-2 overexpression obscured delayed neuronal differentiation
- Evoked neuronal activity is decreased in Ngn2-induced neurons from CUL3 ko iPSC, while spontaneous activity is unchanged
- FGF signaling is affected in CUL3 knockout neural precursor cells, while RhoA and Notch signaling is unaltered

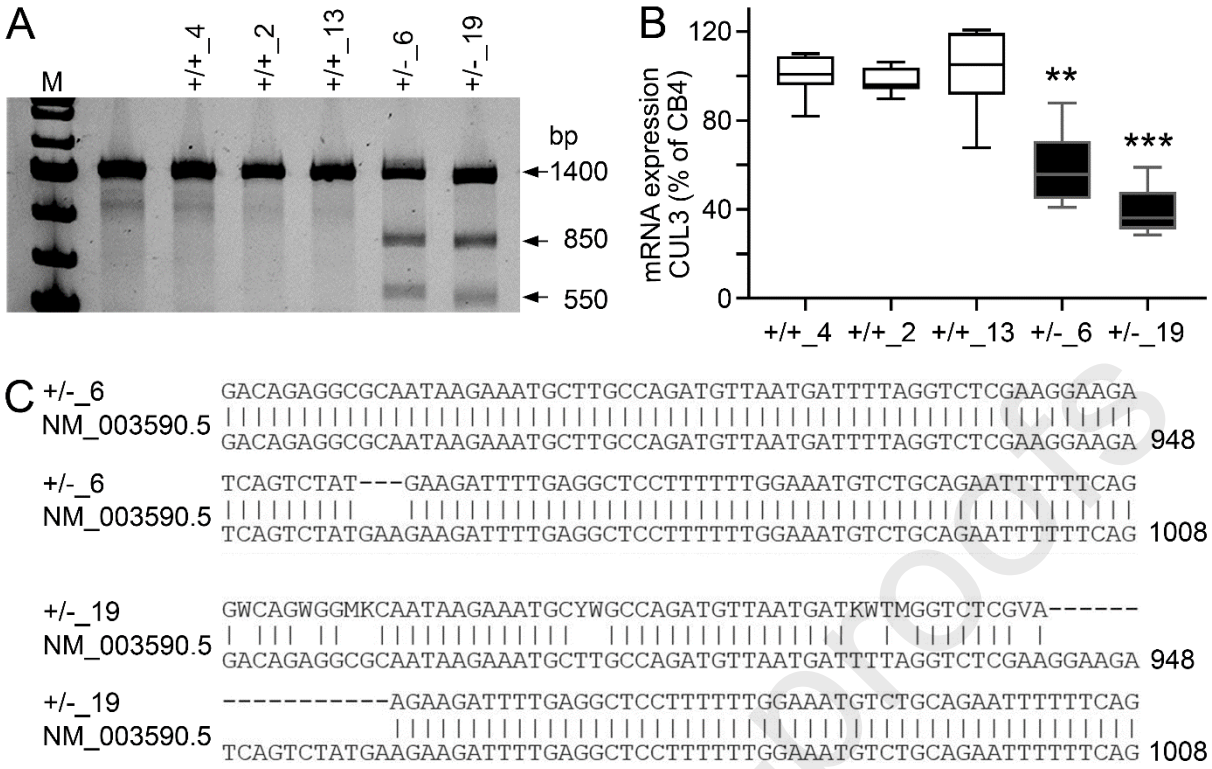

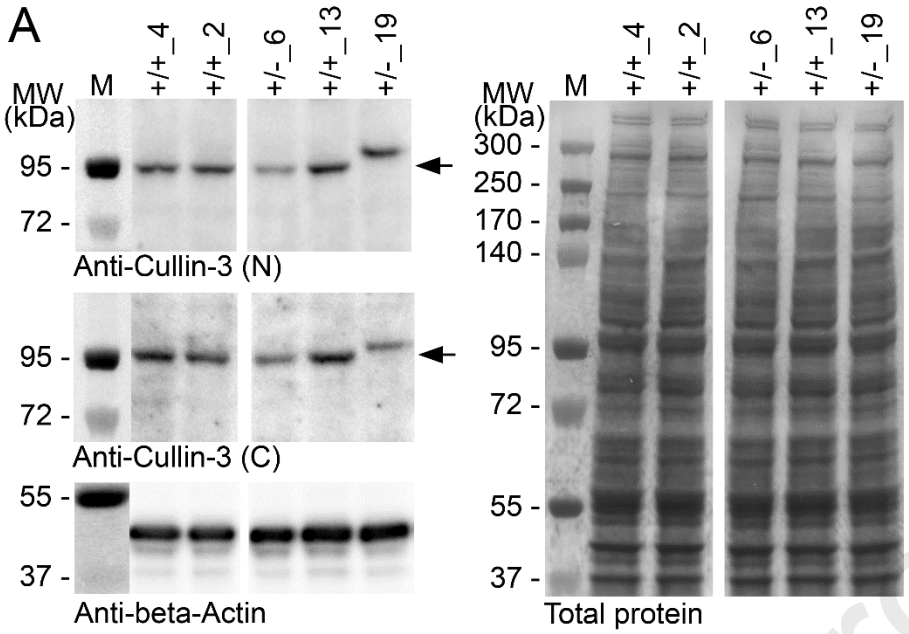

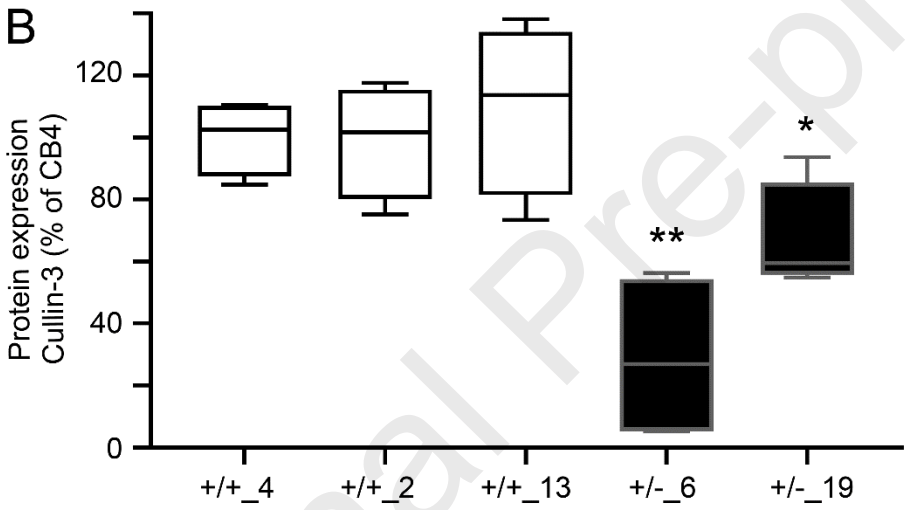

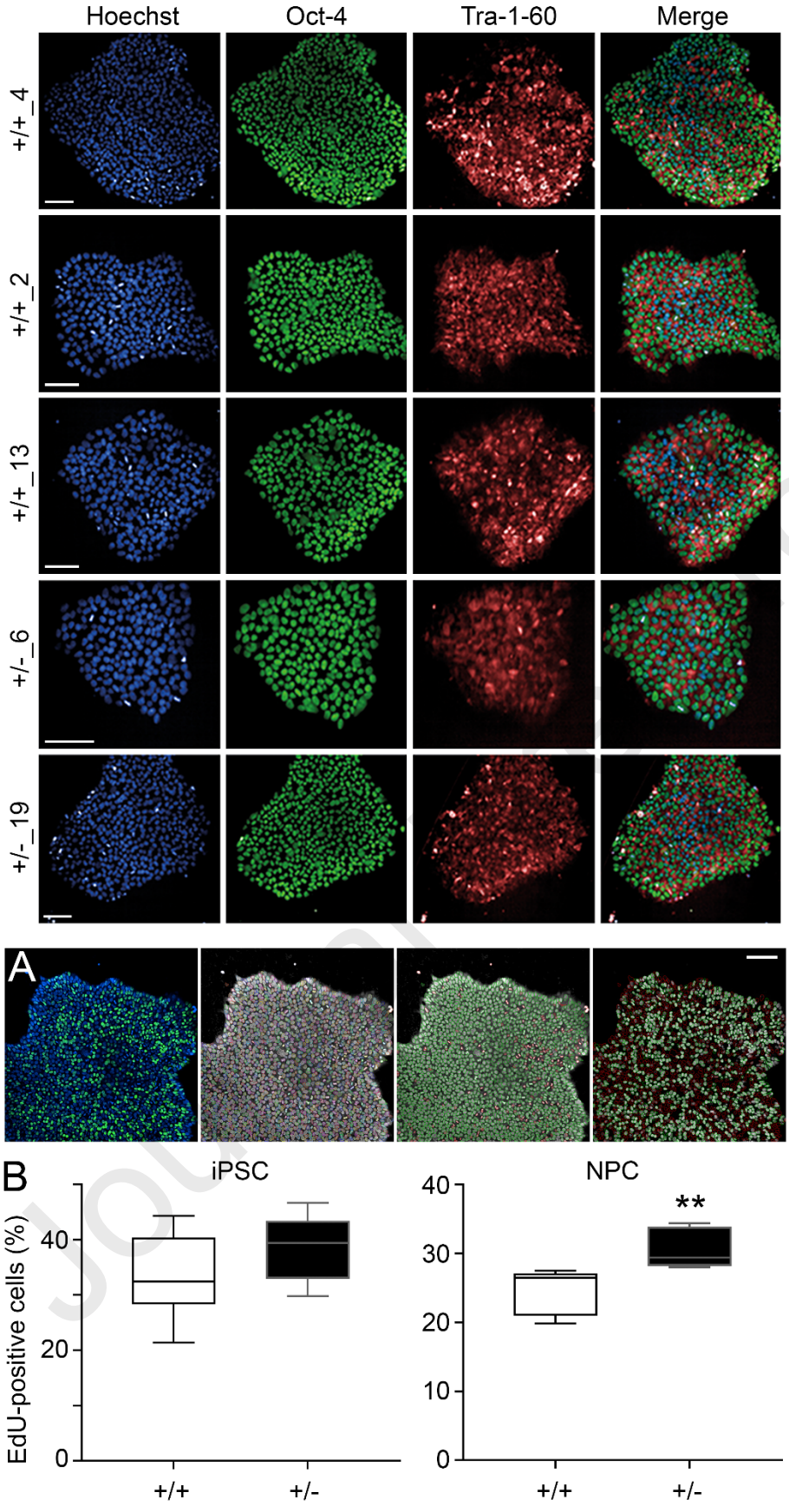
Hoechst
Oct-4
Tra-1-60
Merge
+/+_4
+/+_2
+/+_13
+/-_6
+/-_19
A
B
iPSC
NPC
EdU-positive cells (%)
40
20
0
30
10
**
+/+
+/-

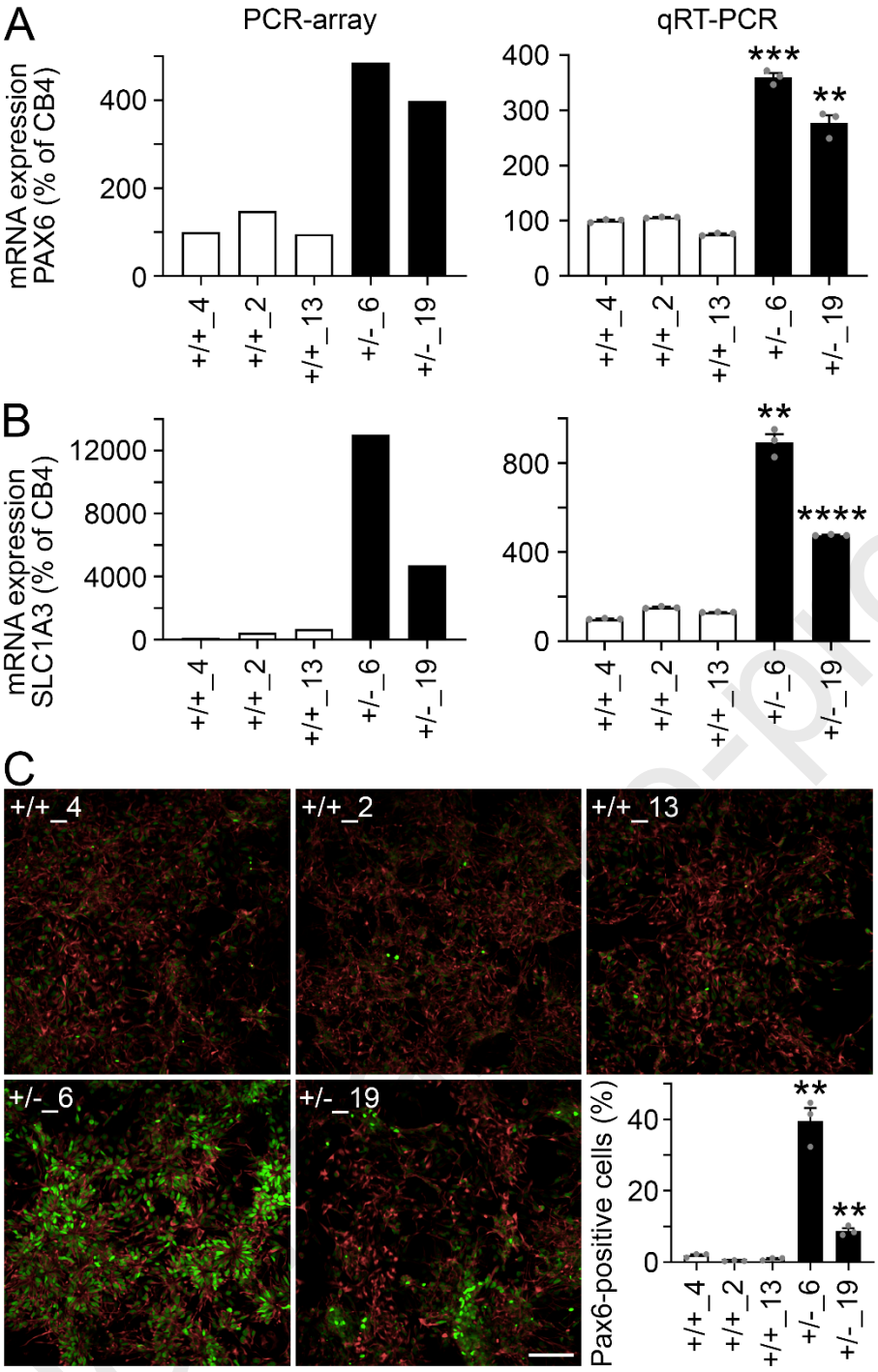

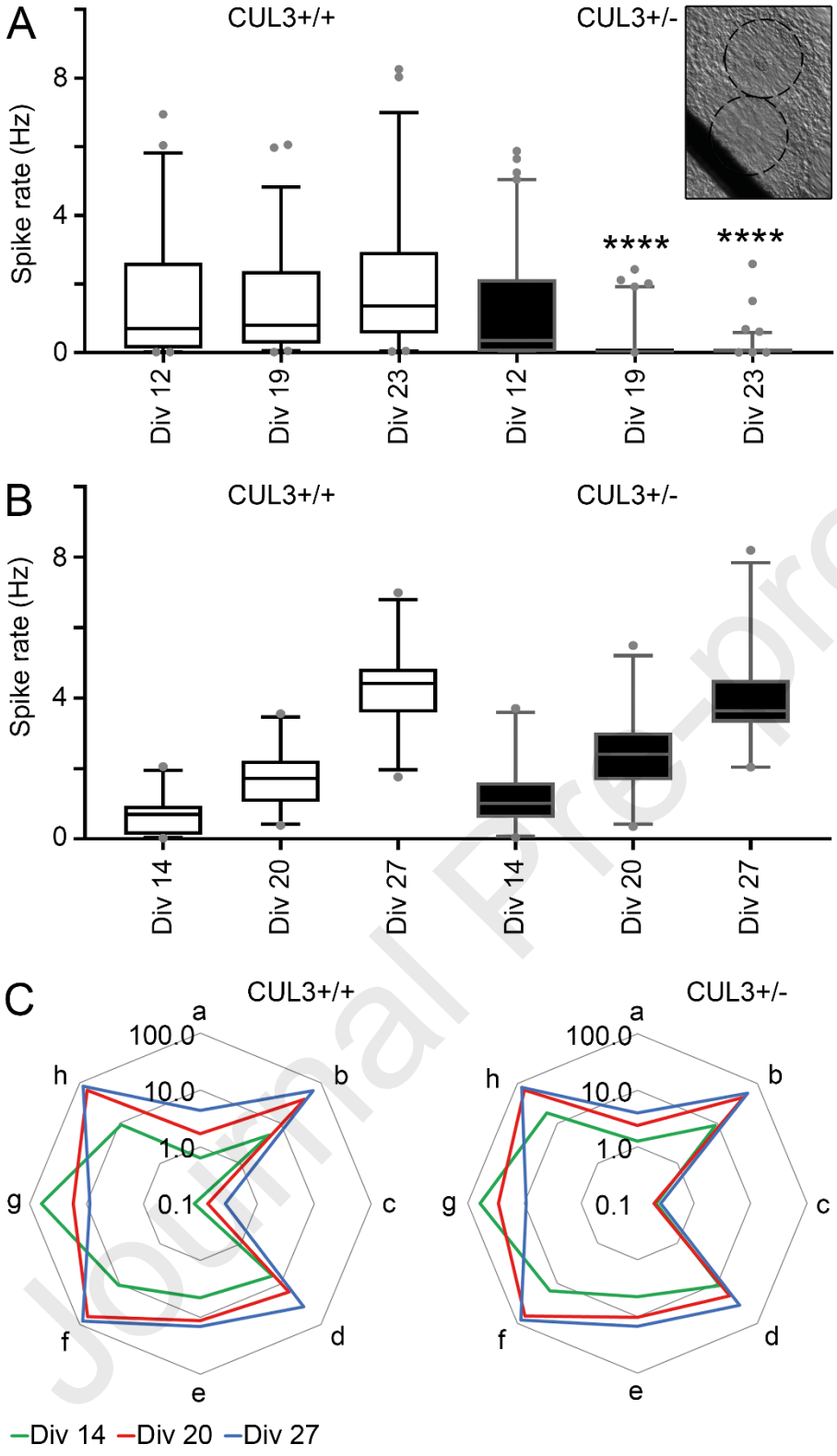

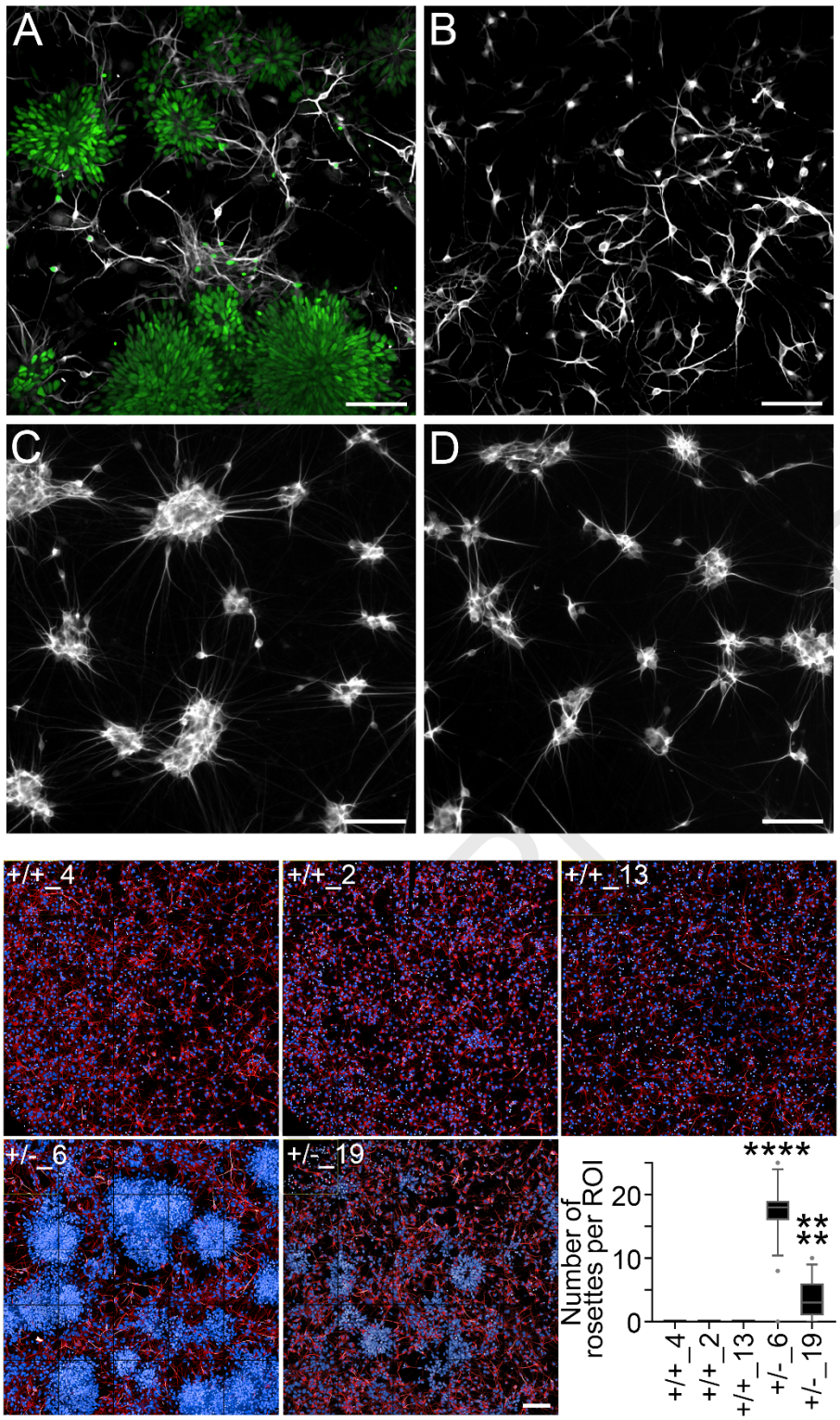
A
B
C
D
+/+_4
+/+_2
+/+_13
+/-_6
+/-_19
Number of rosettes per ROI
0
10
20
****
**
**
+/+_4
+/+_2
+/+_13
+/-_6
+/-_19